

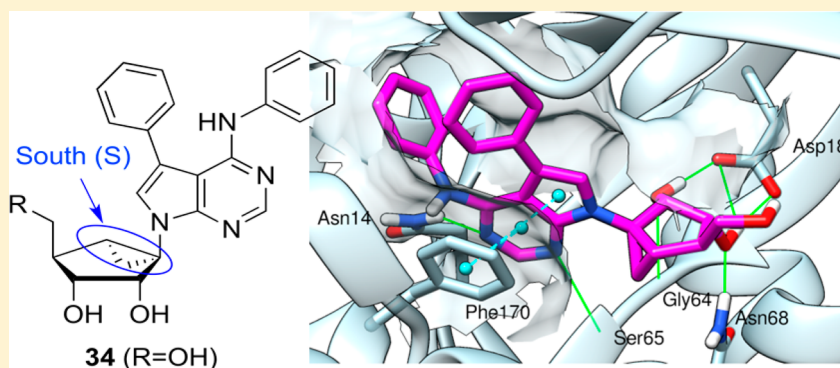
South (S)- and North (N)-Methanocarpa-7-Deazaadenosine Analogues as Inhibitors of Human Adenosine Kinase

Kiran S. Toti,[†] Danielle Osborne,[‡] Antonella Ciancetta,[†] Detlev Boison,[‡] and Kenneth A. Jacobson^{*,†}

[†]Molecular Recognition Section, Laboratory of Bioorganic Chemistry, National Institute of Diabetes and Digestive and Kidney Diseases, National Institutes of Health, Bldg. 8A, Rm. B1A-19, Bethesda, Maryland 20892-0810, United States

[‡]Robert Stone Dow Neurobiology Laboratories, Legacy Research Institute, 1225 NE Second Avenue, Portland, Oregon 97232, United States

S Supporting Information



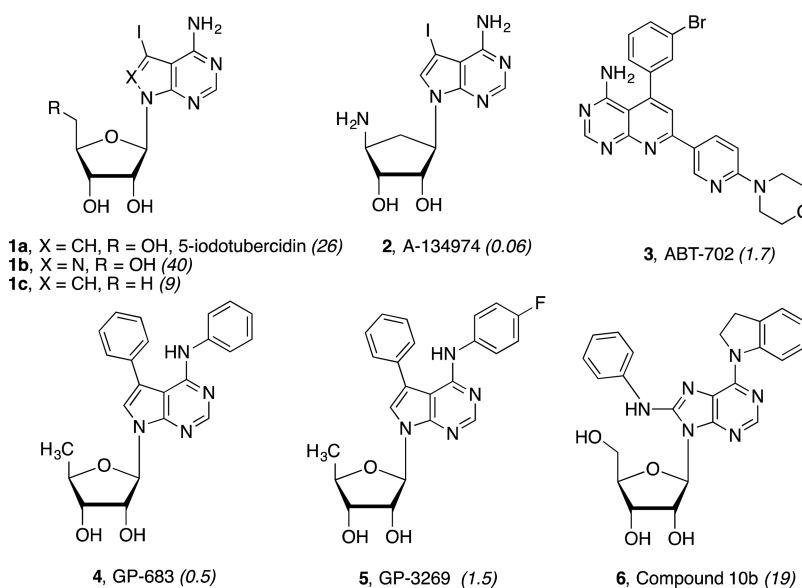
ABSTRACT: Adenosine kinase (AdK) inhibitors raise endogenous adenosine levels, particularly in disease states, and have potential for treatment of seizures, neurodegeneration, and inflammation. On the basis of the South (S) ribose conformation and molecular dynamics (MD) analysis of nucleoside inhibitors bound in AdK X-ray crystallographic structures, (S)- and North (N)-methanocarpa (bicyclo[3.1.0]hexane) derivatives of known inhibitors were prepared and compared as human (h) AdK inhibitors. 5'-Hydroxy (34, MRS4202 (S); 55, MRS4380 (N)) and 5'-deoxy 38a (MRS4203 (S)) analogues, containing 7- and N⁶-NH phenyl groups in 7-deazaadenine, robustly inhibited AdK activity (IC₅₀ ~ 100 nM), while the 5'-hydroxy derivative 30 lacking the phenyl substituents was weak. Docking in the hAdK X-ray structure and MD simulation suggested a mode of binding similar to 5'-deoxy-5-iodotubercidin and other known inhibitors. Thus, a structure-based design approach for further potency enhancement is possible. The potent AdK inhibitors in this study are ready to be further tested in animal models of epilepsy.

INTRODUCTION

Endogenous adenosine acts on its G protein-coupled receptors (adenosine receptors, ARs)¹ in the central nervous system to suppress seizures² and pain³ and to blunt the effects of ischemia.⁴ In addition, adenosine has AR-independent epigenetic effects based on interactions with the transmethylation pathway.⁵ Extracellular adenosine may originate from intracellular pools or from the action of ectonucleotidases on extracellular ATP.⁶ There is a dynamic equilibrium between extracellular adenosine levels and its intracellular content that is mediated by either equilibrative (ENTs) or concentrative (CNTs) transporters of nucleosides.⁷ Within the brain, the concentration of adenosine is largely under the control of metabolic clearance through astrocytic adenosine kinase (AdK), which converts adenosine to 5'-AMP.⁸ AdK exists in two isoforms derived from alternative splicing and alternative promoter use. The short isoform AdK-S resides in the cytoplasm, whereas the long isoform AdK-L is located in the cell nucleus.⁹ By inhibiting AdK, the adenosine concentration can be exogenously raised. Thus, an indirect means of

modulating the concentration of adenosine in the brain, and therefore the basal levels of activation of the ARs, is by administering brain-penetrant human (h) AdK inhibitors. The raised level of adenosine in the brain counteracts seizures by activating the neuroprotective A₁AR and attenuates epilepsy progression by decreasing S-adenosyl methionine dependent DNA methylation as an epigenetic mechanism of action.^{8,10} Increased DNA methylation is a pathological hallmark of chronic epilepsy and associated with disease progression and maintenance of the epileptic state.^{5,11} Efficient transmethylation reactions, for example, in the liver, require the removal of adenosine by AdK,¹¹ and this effect has been demonstrated to occur in the brain as well.^{5,8} Unlike adenosine itself, synthetic A₁AR agonists, which are also proposed for seizure treatment,^{10,13} would not inhibit DNA methylation. Overexpression of AdK in the brain is both a result of astroglial activation and a contributing factor to epileptic seizures. Thus, an inhibitor of

Received: May 5, 2016

Chart 1. Known Nucleoside and Nonnucleoside Inhibitors of hAdK That Have Been Examined in Models of Pain and/or Seizures^a

^aPublished potencies (IC₅₀ values) for inhibition of the hAdK catalysis of the conversion of adenosine to AMP are given in nM.^{7,29}

AdK might have an advantage in seizure control because it would combine a pharmacological mechanism (increased A₁AR activation) with epigenetic mechanisms (decreased DNA methylation) and might preferentially act on pathologically increased AdK as opposed to normal baseline levels of the enzyme. The advantages of “adenosine augmentation therapies” for epilepsy and its associated comorbidities have already been discussed.^{14–16}

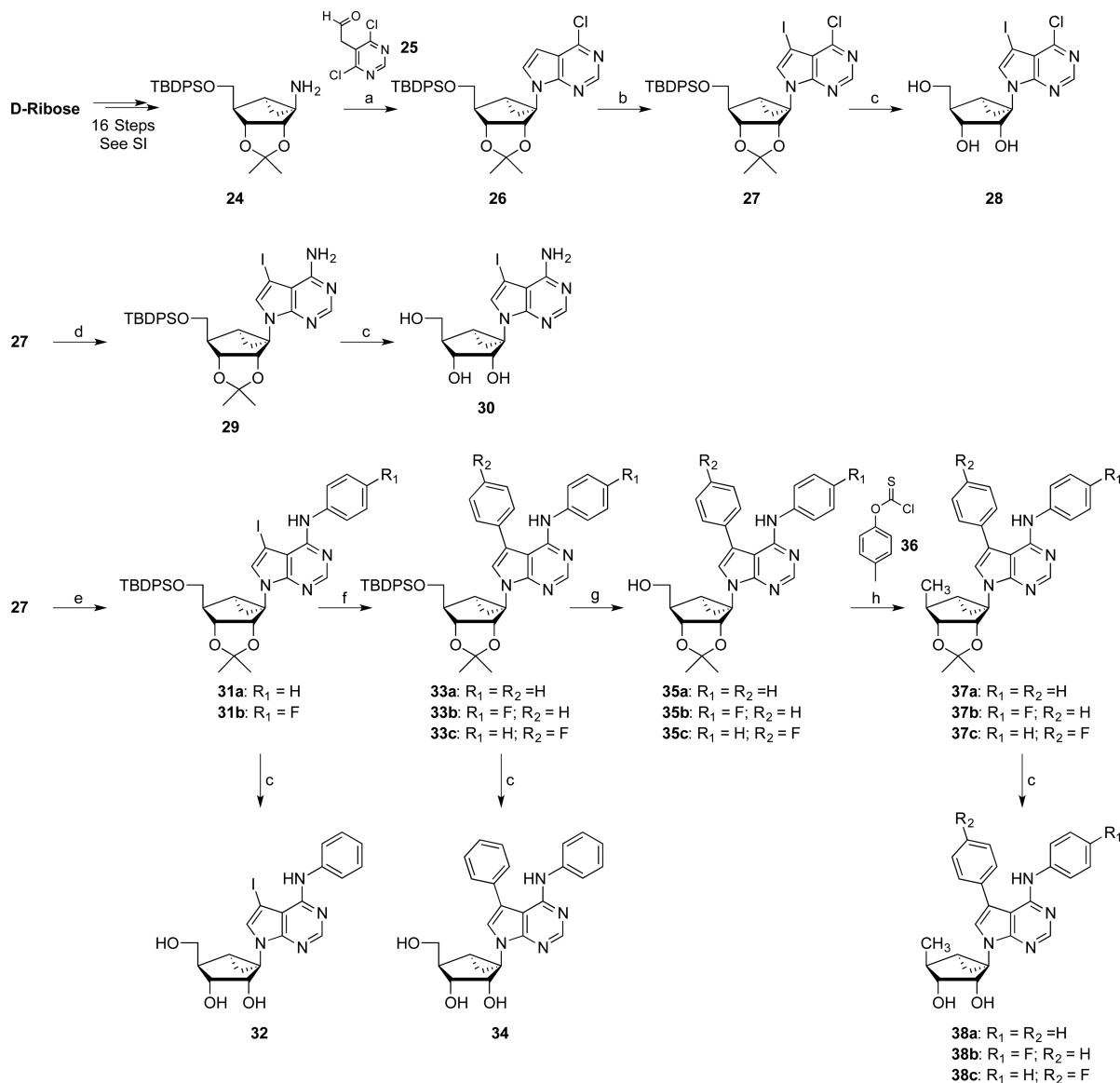
Several classes of AdK inhibitors have already been introduced and explored for the treatment of seizures and pain (Chart 1, 1–6).^{17–21} One class consists of nucleosides derived from the known AdK inhibitor 7-iodo-7-deazaadenosine 1a, otherwise known as 5-iodotubercidin (5-IT). *N*′-[(1′*R*,2′*S*,3′*R*,4′*S*)-2′,3′-Dihydroxy-4′-aminocyclopentyl]-4-amino-5-iodopyrrolopyrimidine (2, A-134974) acts in the spinal cord to reduce carrageenan-induced inflammatory hyperalgesia.²² Both 1a and its potent analogue, e.g., the AdK inhibitor 4-(*N*-phenylamino)-5-phenyl-7-(5′-deoxyribofuranosyl)pyrrolo[2,3-*d*]pyrimidine 4, inhibited maximal electroshock (MES) seizures in rats.² Compound 4 also reduced the volumes of infarction in a model of focal cerebral ischemia in rats.²³ Another class of nonnucleoside, heterocyclic inhibitors includes the widely used AdK inhibitor 4-amino-5-(3-bromophenyl)-7-(6-morpholino-pyridin-3-yl)pyrido[2,3-*d*]pyrimidine (3, ABT-702). Potent and selective inhibitors of the AdK of *Mycobacterium tuberculosis* that do not affect human AdK were found to have antimicrobial activity.^{24,25} AdK inhibitors were being considered for clinical trials for pain and seizure treatment in the early 2000s, but this effort was discontinued, with one of the inhibitors causing brain hemorrhage in dogs.²⁶ Thus, AdK inhibition holds interest for the control of infectious, as well as neurological diseases. AdK inhibitors also induce anti-inflammatory effects that are adenosine-dependent.²⁷ A potent AdK inhibitor, 4-amino-3-iodo-1-β-D-ribofuranosylpyrazolo[3,4-*d*]pyrimidine 1b, was also shown to indirectly reduce the expression of inducible nitric oxide synthase and tumor necrosis factor (TNF) in glial cells via activation by adenosine of G_s-coupled ARs.^{28,29} Recently,

the AdK inhibitor 3 was found to promote rodent and porcine islet β-cell replication, which suggests the possible application of such inhibitors to the treatment of diabetes.³⁰ However, other, undesired effects of the inhibitor 1a have been noted; it seems to indirectly inhibit acetyl-CoA carboxylase to promote oxidation of hepatic fatty acids and reduce de novo synthesis of lipids and cholesterol, which raises the AMP/ATP ratio.³¹ Thus, there might be a need to increase selectivity for AdK within this nucleoside series.

A common approach in medicinal chemistry to enhance the activity or selectivity of flexible biologically active, small molecules is to introduce a conformational constraint to achieve a desired conformation for interacting with a target biopolymer, i.e., here an enzyme. This lowers the energy barrier of the binding process and can eliminate undesired interactions with other molecular targets that prefer a different conformation of the ligand. One means of sterically constraining the ribose ring of nucleoside derivatives, as already applied to antiviral agents and to receptor ligands, is to incorporate a bicyclic ribose substitute in a conformation that is preferred when the molecule is bound to the protein target.^{32,33} The methanocarba ([3.1.0]bicyclohexane) ring system is applied to hold the ribose-like ring in either a North (N) or a South (S) conformation. The X-ray structure of human AdK shows a bound nucleoside inhibitor 1c containing a ribose in the (S) conformation, which is similar to the ribose conformation preferred by other nucleoside kinases.^{34–37} This prompted us to explore the effects of sterically constraining nucleoside inhibitors of human AdK using methanocarba rings.

RESULTS

Chemical Synthesis. The intermediate 24 containing the (S)-methanocarba ring with 1′-amino functionalization was required as an intermediate for the target compounds (Scheme 1). We adapted our previously reported synthesis of enantiomerically pure (S)-methanocarba nucleosides via bicyclic intermediate 24^{38,39} to a larger scale preparation of this intermediate (Supporting Information, Scheme S1).

Scheme 1. Synthesis of Nucleobase Modified (S)-Methanocarba Analogues of 5-Iodotubercidin⁴⁴

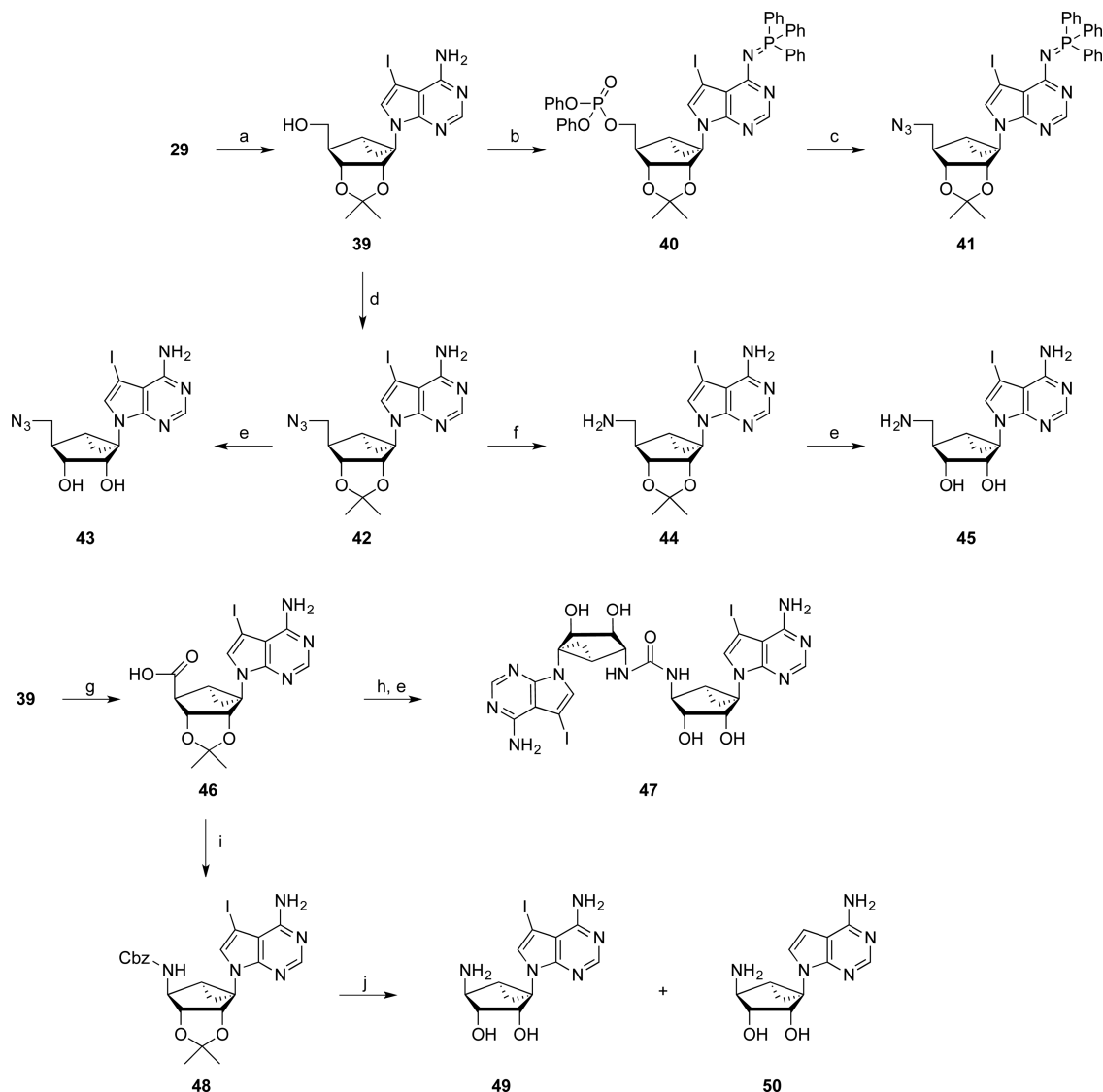
⁴⁴Reagents and conditions: (a) EtOH, 2-(4,6-dichloropyrimidin-5-yl)acetaldehyde (**25**), NEt₃, reflux, 18 h, 76%; (b) anhydrous DMF, NIS, 60 °C, 6 h, 92%; (c) 70% TFA (aq), rt, 1.5 h, from **27**, 83%; (d) EtOH, 7N NH₃-MeOH, sealed tube, 110 °C, 18 h, 89%; (e) anhydrous THF, aniline, 1M tBuOK in THF, -20 °C, 1.5 h, 70–80%; (f) 6:1 DME-EtOH, phenylboronic acid, Pd(PPh₃)₄, satd Na₂CO₃ (aq), 90 °C, 7 h, 75–86%; (g) anhydrous THF, 1M TBAF in THF, rt, 18 h, 85–96%; (h) (i) anhydrous CH₃CN, DMAP, *O*-(*p*-tolyl) chlorothionoformate (**36**), rt, 18 h, (ii) anhydrous toluene, Bu₃SnH, AIBN, reflux, 2 h, 52–90%.

Using the (S)-methanocarba intermediate **24** as a precursor, analogues of known AdK nucleoside inhibitors were prepared. The 7-deazaadenine core was constructed by reacting **24** with symmetrical dichloropyrimidine bearing an acetaldehyde moiety (**25**),⁴⁰ which on iodination using NIS followed by the removal of protecting groups in aqueous trifluoroacetic acid resulted in **28**. Similarly, the aminolysis of **27** and deprotection rendered **30**, the (S)-methanocarba analogue of **1a**, in moderate yield.

Substitution of chlorine on the 6-position of 7-deazapurine using aniline and sodium acetate achieved a complete reaction, but the use of a stronger base, i.e., potassium *tert*-butoxide at lower temperature produced N⁶-phenyl 7-iodo derivatives **31a** and **31b** in increased yields. A Suzuki reaction involving arylboronic acids and **31a,b**, followed by the removal of a silyl protecting group, gave **35a–c**, which were subjected to

Barton–McCombie deoxygenation⁴¹ to yield 5'-deoxy compounds **37a–c**. Removal of the protecting groups from **31**, **33**, and **37a–c** gave **32**, **34**, and **38a–c**, respectively, in low to moderate yields.^{17,42} Compounds **38b** and **38c** differ from **38a** only in the presence of a fluorine atom in the *p*-position of either the 4-phenyl-amino or 5-phenyl ring, respectively.

In an attempt to synthesize 5'-azido compounds (Scheme 2), a Mitsunobu reaction involving diphenylphosphoryl azide (DPPA) and **29** yielded disubstituted **40** exclusively. Surprisingly, this compound was sufficiently stable to be isolated using silica gel column chromatography. **40** on heating with sodium azide in DMF formed undesired product **41**, and attempts to convert this phosphine to **42** or **43** using aqueous TFA were unsuccessful. Alternatively, mesylation of **29** followed by substitution with sodium azide at elevated temperature afforded the desired compound **42** in 96% yield, which under Staudinger

Scheme 2. Synthesis of 4'-Position Modified (S)-Methanocarba Analogues of 5-Iodotubercidin^a

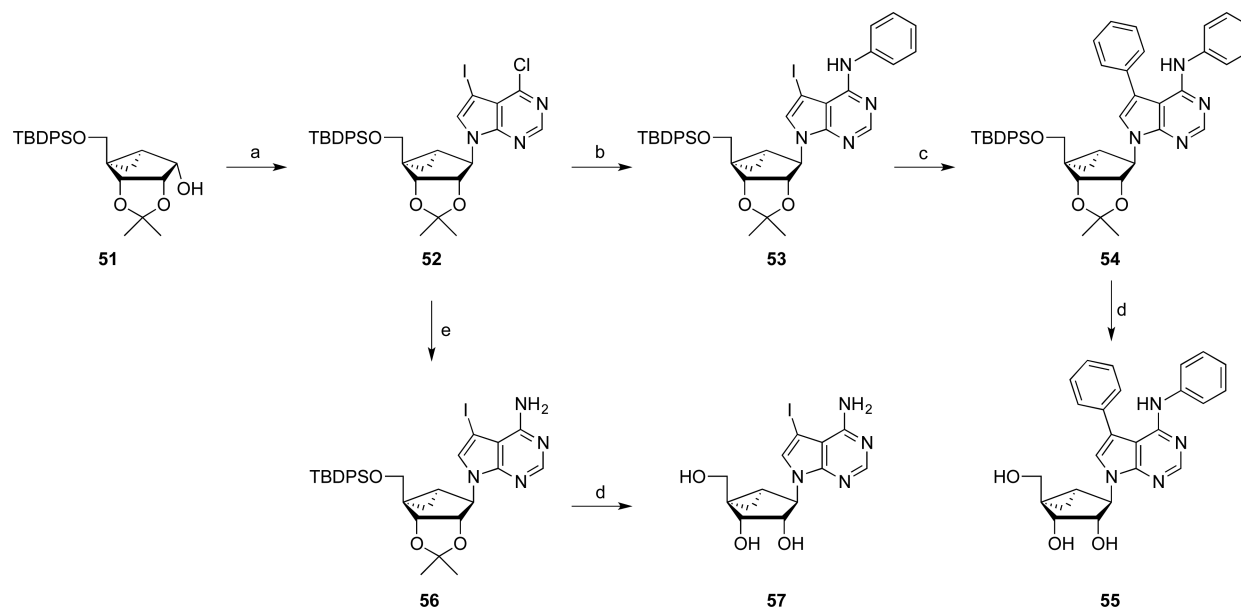
^aReagents and conditions: (a) anhydrous THF, 1M TBAF in THF, rt, 18 h, quantitative yield; (b) anhydrous THF, PPh₃, DEAD, DPPA, 0 °C → rt, 18 h; (c) anhydrous DMF, NaN₃, 65 °C, 24 h; (d) (i) anhydrous pyridine, MsCl, 0 °C → rt, 4 h, (ii) anhydrous DMF, NaN₃, 65 °C, 4 h, 95%; (e) 70% TFA (aq), rt, 1.5 h, 35–42%; (f) (i) anhydrous THF, PPh₃, rt, 18 h, (ii) 25% NH₄OH (aq), 65 °C, 4 h, 80%; (g) 4:1 CH₃CN–H₂O, BAIB, TEMPO, rt, 18 h, 49%; (h) DPPA, TEA, anhydrous *t*-BuOH, rt, 30 min, 90 °C, 2 h; (i) (i) DPPA, TEA, anhydrous THF, rt, 18 h, (ii) toluene, benzyl alcohol, 110 °C, 5 h, 17%; (j) anhydrous CH₂Cl₂, 33% HBr–CH₃COOH, 0 °C → rt, 2.5 h, 17%.

reaction conditions gave **44** in good yield.⁴³ The deprotection of the acetonide group from **42** and **44** using aqueous TFA led to 5'-azido and 5'-amino congeners **43** and **45**, respectively.

To arrive at **49** from **39**, a Curtius rearrangement strategy was adapted, and to realize this, the 4'-hydroxymethyl group in **39** was converted to the corresponding carboxylic acid **46** employing a TEMPO-BAIB oxidation⁴⁴ in aqueous acetonitrile. Initial efforts to prepare the Boc-protected analogue of urethane **48** from **46** using DPPA and *tert*-butanol failed, but instead, after deprotection of the isopropylidene group, resulted in dimer **47**. However, a similar reaction with benzyl alcohol formed Cbz-protected compound **48**,³⁹ which on deprotection using 33% HBr in acetic acid provided the desired compound **49**, as a minor product, and **50** as the major product. Unfortunately, an attempt to convert **50** to the desired compound **49** using NIS in DMF at elevated temperature did not materialize.

The synthesis of several corresponding (N)-methanocarba analogues was performed as shown in Scheme 3. A protected bicyclic intermediate **51**, prepared previously for studies of adenosine receptors,^{38,39,45} was subjected to a Mitsunobu reaction with 6-chloro-7-iodo-7-deazapurine. The next step provided two divergent pathways leading to target inhibitors: nucleophilic substitution of the 4-chloro group with either ammonia or aniline (followed by a Suzuki coupling at the 5-position). Deprotection of the hydroxyl groups yielded compounds **55** and **57**, which are the (N)-methanocarba equivalent of compounds **34** and **30**, respectively.

Biochemical Evaluation. The nucleoside derivatives were tested for inhibitory potential at hAdK using a commercial, nonisotopic assay for the measurement of hAdK activity based on continuous monitoring at 340 nm (appearance of reduced nicotinamide-adenine dinucleotide from a coupled enzymatic reaction). The hAdK-catalyzed phosphorylation of inosine to

Scheme 3. Synthesis of (*N*)-Methanocarba Analogue 57 of 5-Iodotubercidin and Its *N*⁶,7-Diphenyl Congener 55^a

^aReagents and conditions: (a) 6-chloro-7-iodo-7-deazapurine, anhydrous THF, DEAD, PPh₃, 0 °C → rt, 18 h, 88%; (b) anhydrous THF, aniline, 1M tBuOK in THF, −20 °C, 1.5 h, 63%; (c) 6:1 DME–EtOH, phenylboronic acid, Pd(PPh₃)₄, satd Na₂CO₃ (aq), 90 °C, 7 h, 82%; (d) 70% TFA (aq), rt, 1.5 h, 77–79%; (e) EtOH, 7N NH₃–MeOH, sealed tube, 110 °C, 18 h, 82%.

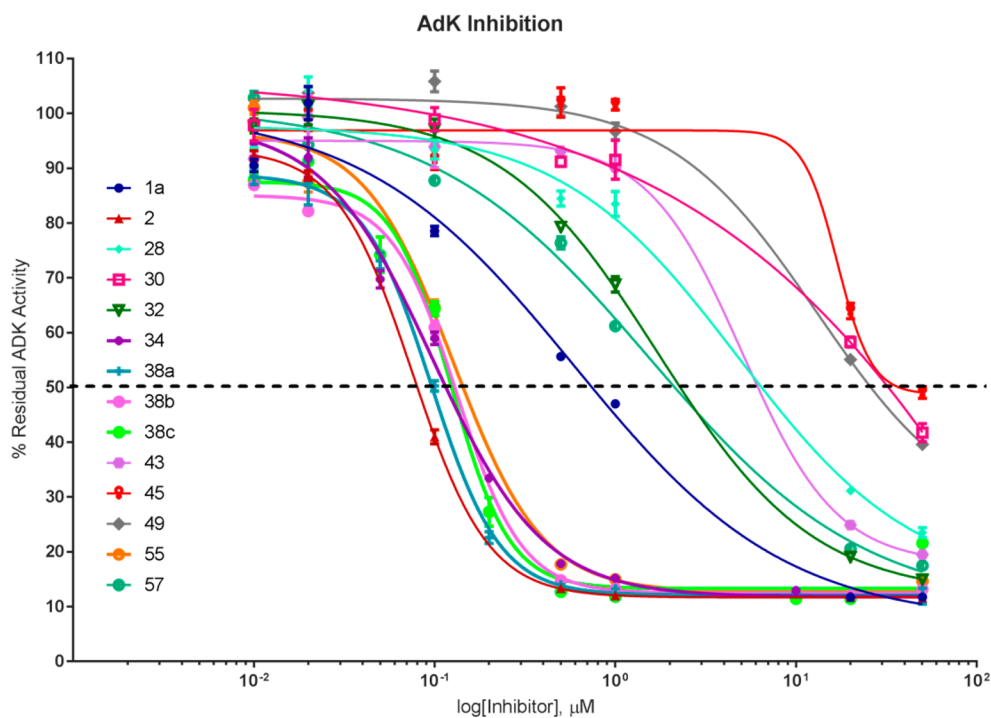


Figure 1. Concentration–response study for all inhibitors compared to **1a** and **2** at 50 μM, 20 μM, 1 μM, 500 nM, 100 nM, 20 nM, and 10 nM. Percent residual activity of **38a** was commensurate with **2** at most concentrations. Slope activity was determined between 0 and 40 min of assay activity time and determined as a percentage relative to DMSO.

inosine 5′-monophosphate is coupled to the inosine 5′-monophosphate dehydrogenase-dependent oxidation of the product. Thus, the assay was performed in the presence of dithiothreitol, oxidized nicotinamide-adenine dinucleotide (NAD, 2.5 mM) and ATP (2.75 mM) as cofactors and inosine (2.5 mM) as substrate. hAdK activity was continuously measured via absorption at 340 nm for 4 h, where measurements were made at 5 min intervals; however, for

graphing and analysis purposes, we focused on the first 40 min, which was mostly linear, for determining the slope of initial AdK activity (Figure 1). Percent inhibition of hAdK activity was calculated by determining the change in the slope of the hAdK reaction in the absence or presence of inhibitor during the linear phase of the enzymatic reaction (first 40 min) (Table 1). We included two known AdK inhibitors, compound **1a** and **2**, as positive controls. Each inhibitor was analyzed at the

Table 1. Percent Inhibition of hAdK Activity for All 14 Inhibitors, Relative to Uninhibited Activity, At Concentrations of 50 μ M, 20 μ M, 500 nM, and 100 nM, and the Derived IC₅₀ Values

Compound	Inhibition at concentration indicated, ^a mean % \pm SEM				IC ₅₀ (μ M) + SEM
	50 μ M	20 μ M	500 nM	100 nM	
Control	0	0	0	0	ND
1a, 5-IT	88.3 \pm 0.3	88.3 \pm 0.3	44.4 \pm 0.8	21.5 \pm 0.9	0.82 \pm 0.03
2	88.4 \pm 0.3	88.3 \pm 0.3	86.7 \pm 0.2	59.0 \pm 1.3	0.048 \pm 0.001
(S)-Methanocarba nucleosides					
28	76.5 \pm 0.9	68.9 \pm 0.8	15.6 \pm 1.4	6.6 \pm 1.7	6.01 \pm 0.18
30	58.2 \pm 1.7	41.7 \pm 0.9	8.8 \pm 0.9	1.1 \pm 2.1	ND
32	85.1 \pm 0.6	80.9 \pm 0.2	20.7 \pm 0.8	2.9 \pm 1.9	3.34 \pm 0.19
34	88.3 \pm 0.4	88.1 \pm 0.3	82.2 \pm 0.4	41.0 \pm 1.2	0.114 \pm 0.002
38a	88.1 \pm 1.5	88.4 \pm 0.4	86.0 \pm 0.3	49.7 \pm 1.0	0.088 \pm 0.003
38b	86.9 \pm 0.3	88.0 \pm 0.3	85.2 \pm 0.3	39.0 \pm 1.2	0.110 \pm 0.003
38c	78.4 \pm 0.7	88.6 \pm 0.2	87.3 \pm 0.3	35.6 \pm 1.3	0.115 \pm 0.005
43	80.5 \pm 0.8	75.1 \pm 0.5	6.8 \pm 0.7	6.1 \pm 3.8	5.38 \pm 0.10
45	50.9 \pm 1.1	36.0 \pm 1.4	-2.0 \pm 2.7	8.4 \pm 1.9	ND
49	60.4 \pm 0.8	44.9 \pm 0.7	-1.3 \pm 1.7	-5.8 \pm 2.0	ND
(N)-Methanocarba nucleosides					
55	85.4 \pm 0.5	88.0 \pm 0.2	82.3 \pm 0.5	35.5 \pm 1.4	0.14 \pm 0.01
57	82.5 \pm 0.3	79.5 \pm 0.4	23.6 \pm 1.1	12.3 \pm 0.4	2.24 \pm 0.04

^aBased on slope of the linear portion (0–40 min interval) of the activity plot of hAdK, compared to control with DMSO vehicle. ND, not determined.

following concentrations (μ M): of 50, 20, 1, 0.50, 0.10, 0.020, and 0.010. Percent residual hAdK activity showed a significant interaction ($F_{78490} = 71$, $p < 0.0001$) and main effects for both inhibitor ($F_{13490} = 626$, $p < 0.0001$) and concentration ($F_{6490} = 3366$, $p < 0.0001$). Post hoc analysis used Bonferroni multiple comparison tests to determine drug differences relative to **2** (most potent known inhibitor used here) at each of the concentrations investigated. At the highest concentration, **28**, **30**, **45**, **49**, and **57** significantly varied from **2** with poor inhibition of hAdK. Compound **43** was slightly more potent, varying from **2** at 20 μ M. **32** and **55** were moderately potent, beginning to vary from **2** at 1 μ M and 500 nM, respectively. Only at a concentration of 100 nM did the inhibition by **34**, **38b**, and **38c** differ from **2**, while **38a** never significantly varied from **2**, indicating that **38a** as low as 20 nM was equipotent to **2** in inhibition of hAdK. At lower concentrations, **34** and **38a** maintained more potent hAdK inhibition; therefore, it was necessary to determine full concentration–response curves to distinguish between the most potent compounds. We performed a detailed concentration–response study of most of the analogues for precise determination of IC₅₀, using the earlier data with the addition of three concentrations (10, 0.20, and 0.050 μ M). The IC₅₀ values for potent (S)-methanocarba inhibitors **34** and **38a** were 114 and 88 nM, respectively.

Because the 5'-OH derivative **30** was a poor inhibitor of hAdK, we hypothesized that it might serve as a substrate for hAdK, unlike the corresponding riboside **1a**, which is not primarily a substrate.^{29,43} The K_m of adenosine as substrate of hAdK is 700 nM,²⁹ and the nucleoside analogue concentrations that we used in inhibition experiments far exceeded that concentration. By comparison in another kinase system, (S)-methanocarbothymidine, but not (N)-methanocarbothymidine, is a good substrate for herpes simplex virus type 1 thymidine kinase.³⁵ Moreover, (S)-methanocarbothymidine is not a substrate for human cytosolic thymidine kinase isoenzyme 1.³⁵ Thus, it was important to probe the substrate qualities of compound **30**, (S)-methanocarbaadenosine derivative, at hAdK. Therefore, we performed three different assays under similar conditions: first, with substrate in the presence of 1 μ M **30**; second, without substrate in the presence of 1 μ M **30**; and third as a control, without **30**. After 4 h incubation, the resulting mixtures were studied using LC-MS in negative and positive mode (Supporting Information), which could identify and qualitatively measure the levels of nucleosides and their phosphorylated products. In the first and last cases, we detected the final enzymatic product, i.e., xanthosine-5'-phosphate (MW 364 + 1). However, in the first two cases, we found no evidence from the LC-MS analysis that **30** serves as a substrate of hAdK. There was a prominent signal (MW 402 + 1) from unchanged compound **30**, and no detectable or prominent signal of the corresponding 5'-phosphate (MW 482 \pm 1).

Molecular Modeling. The selection of novel AdK inhibitors was informed using molecular modeling studies. To date, three X-ray structures of the hAdK in complex with both nucleoside and nonnucleoside inhibitors have been solved, which revealed at least two different enzyme conformations. A closed form was present in the complexes of hAdK with nucleoside **1c**³⁶ (PDB ID 2I6A) and 7-ethynyl-7-deazaadenosine³⁴ (PDB ID 4O1L), but the enzyme adopted an open conformation in the complex with a bulkier alkynylpyrimidine inhibitor³⁶ (PDB ID 2I6B). Given the structural similarity of our compounds to **1c**, we used the corresponding cocrystallized structure as macromolecular starting point of our analysis.

MD Simulation of the X-ray Structure of the 1c-AdK Complex. In a first instance, we subjected the experimentally determined complex (PDB ID 2I6A) to 30 ns of all atom molecular dynamics (MD) simulation, in order to identify the residues mostly involved in the interaction and to explore in detail the conformational space of the inhibitor. In the starting structure,³⁶ **1c** bound with the glycosidic bond (χ) in the *anti* conformation ($\chi = -134.7^\circ$) and the sugar moiety in the C1'-*exo* conformation ($P = 125.3^\circ$). The analysis of the trajectory (Supporting Information, Video S1, left panel) revealed that the *anti* conformation was retained throughout the simulation, while the pseudosugar ring explored different conformational states (Supporting Information, Figure S2). The *anti* conformation of the glycosidic bond seemed to be compatible with the charge distribution of the residues surrounding the enzyme active site. Indeed, the inhibitor established persistent H-bond interactions with negatively charged residues through the C2' and C3' hydroxyl groups and a stable π - π stacking interaction with Phe170 through the purine core. Moreover, the inhibitor was anchored in the active site of the enzyme through a network of H-bond interactions consisting of the N3 atom of the purine core and the C2' hydroxyl groups associating with the backbone of Ser65 and Gly64, respectively. Concerning the ribose ring conformations of **1c**, the starting

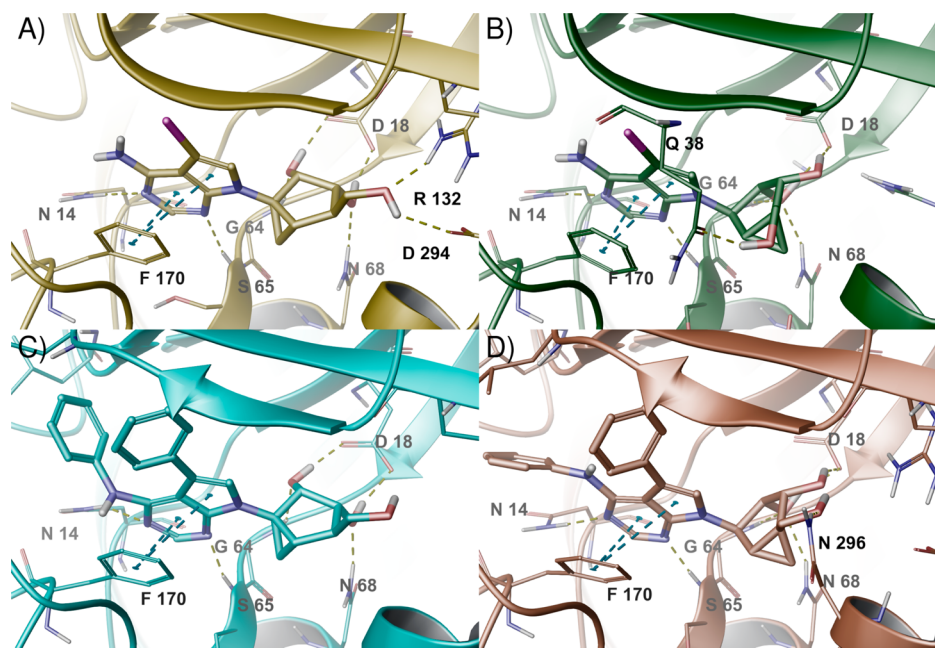


Figure 2. Docking poses of the selected methanocarba derivatives in complex with the closed form of hAdK (PDB ID 2I6A) obtained after IFD: **30** (A) and **57** (B), both derivatives of prototypical AdK inhibitor **1a**; **34** (C) and **57** (D), both containing two phenyl rings. Ligand and side chains of residues important for ligand recognition are represented as line and sticks, respectively. H-Bonds are pictured as yellow dashed lines, while π - π stacking interactions are indicated by blue dashed lines, with the centroids of the aromatic rings displayed as cyan spheres. Nonpolar hydrogen atoms are omitted.

C1'-*exo* conformation (Supporting Information, Figure S2(i)), featuring a bidentate H-bond interaction between the C2' and C3' hydroxyl groups and the side chain of Asp18 (Supporting Information, Video S1), was the most favorable in terms of ligand-protein interaction energy (IE) during the simulation (right panel in Video S1 and upper panel in Supporting Information, Figure S2). However, after approximately 12 ns of MD simulations, the H-bond network was lost and the sugar ring adopted a C2'-*endo* (S) conformation ($P = 156.7^\circ$, Supporting Information, Figure S2 (ii)) with the C2' and C3' hydroxyl groups interacting with the Asp18 side chain and water molecules, respectively (Supporting Information, Video S1). At the end of the simulation (Supporting Information, Video S1), the ring adopted a less favorable, in terms of IE, C3'-*endo* (N) conformation ($P = 36.4^\circ$, Supporting Information, Figure S2 (iii)) that was accompanied by a rotameric switch of the Asp18 side chain to establish a bidentate H-bond interaction with Arg132 while still interacting with the C3' hydroxyl group (data not shown). To assess whether this conformation was persistent, we restarted the simulation for another 30 ns in which the inhibitor remained in the (N) conformation (Supporting Information, Figure S2). These results prompted us to consider nucleoside inhibitors constrained by the methanocarba ring system in the (N) as well as the (S) conformation. We therefore analyzed from a molecular point of view two isomeric pairs by inspecting in detail the comparison between **30** and **57** and between **34** and **55**.

Docking of Selected Methanocarba-Nucleoside Derivatives. The compounds were docked into the closed form of hAdK by using the induced fit docking (IFD) procedure (see Methods section), because a preliminary attempt to dock bulky diphenyl derivatives **34** and **55** into the rigid enzyme in the closed form failed. In all four docking poses (Figure 2), the purine core established a π - π stacking interaction with Phe170 and H-bond interactions with the side chain of Asn14 and the

backbone of Ser65, through the N1 and N3 atoms, respectively. Furthermore, the phenyl rings of **34** and **55** (Figure 2C,D) interacted with residues located in the small lid domain (Leu16, Leu40, Leu134, Ala136, Leu138, and Val174) by means of extended hydrophobic contacts. In the derivatives in the (S) conformation (**30** and **34**, parts A and C of Figure 2, respectively), the methanocarba ring was involved in a tight network of H-bond interactions. The backbone NH of Gly64 and side chain of Asn68, respectively, served as H-bond donors to the C2' and C3' hydroxyl groups. This coordination contributed to placing the same hydroxyl groups in a favorable orientation to act as H-bond donors in a bidentate interaction with the side chain of Asp18. Moreover, several additional H-bond interactions involving the C5' hydroxyl group further stabilized this proposed binding mode. However, in the docking poses of the (N) derivatives (**57** and **55**, parts B and D of Figure 2, respectively), we detected a slightly different interaction pattern to compensate for the loss of the bidentate interaction with Asp18. In particular, the hydroxyl groups at C2' engaged in H-bond interactions with Gly64 (backbone) and Asn68, while the hydroxyl group at C5' established a H-bond interaction with the side chain of Gln38 and with Asn296 in the docking pose of **57** and **55**, respectively. As shown below, this different orientation of the (N) isomer was constrained by the closed form of the rigid enzyme and the bidentate interaction was partially restored by relaxing the protein in a dynamic environment.

MD Simulations of Methanocarba-Nucleoside hAdK Complexes. The docking poses described above were subjected to 30 ns of all-atom MD simulation. The visualization of the trajectory of the comparison between the **30**-hAdK and **57**-hAdK complexes (Supporting Information, Video S2), revealed that in the **30**-hAdK complex (Supporting Information, Video S2, left panel), the H-bond interaction network anchoring the C2' and C3' hydroxyl groups in a favorable orientation to

establish a bidentate interaction with Asp18 side chain was lost after approximately 14 ns. This conformational change followed the opening of the small lid domain, probably triggered by the steric hindrance imposed by the fused three-membered ring. However, in the trajectory of the 57-hAdK complex (Supporting Information, Video S2, right panel), the H-bond network was maintained throughout the simulation. A comparison of trajectories of the 34-hAdK and 55-hAdK complexes (Supporting Information, Video S3) highlighted the almost immediate opening of the small lid domain for both complexes. This opening established π - π stacking interactions between Phe170 (purine core) and Phe201 (phenyl-amino group) and van der Waals interactions with the side chains of Gln38 (phenyl group, data not shown), Leu40, and Leu138 (phenyl-amino group), which persisted throughout the simulation. In the 34-hAdK complex (Supporting Information, Video S3, left panel), the C2' and C3' hydroxyl groups and the Asp18 side chain persisted in a reciprocal favorable orientation for almost the entire duration, through the interplay of Asp300, Arg332, and water molecules. The analysis of the trajectory of the 55-hAdK complex (Supporting Information, Video S3, right panel), indeed, featured less enduring H-bond networks and more predominant van der Waals interactions that contributed to a net IE profile that was slightly more favorable (Supporting Information, Figure S3).

hAdK Conformation during MD Simulations. As mentioned above, initial attempts to dock the 34 and 55 in the closed conformation of the enzyme failed. We therefore resorted to an IFD protocol to obtain initial docking poses that we subsequently subjected to MD simulation (30 ns). The analysis of the trajectories revealed that the opening of the small lid domain occurred after a few ns of simulation for the hAK complexes with 34 and 55 (Supporting Information, Video S3, left and right panels) and after approximately 14 ns of simulation for the 30-hAK complex (Supporting Information, Video S2, left panel). Superimposition of MD average protein structures with respect to the enzyme starting structure (PDB ID 2I6A, gray ribbons) is depicted in Supporting Information, Figure S4. First, we compared the X-ray structures of the enzyme in the closed conformation (PDB ID 2I6A, gray ribbons in Supporting Information, Figure S4) and the open conformation (PDB ID 2I6B, green ribbons in Supporting Information, Figure S4A). Comparing each MD average structure with the starting conformation highlighted that the enzyme remained in the closed conformation for the hAdK complexes with 1c (Supporting Information, Figure S4B, pink ribbons) and 57 (Supporting Information, Figure S4D, green ribbons). However, in the complexes with 30 (Supporting Information, Figure S4C, yellow ribbons), 34 (Supporting Information, Figure S4E, cyan ribbons), and 55 (Supporting Information, Figure S4F, orange ribbons), the enzyme approached the open conformation. In particular, in the MD average structures, the small lid domain was rotated outward by about 24° with respect to the large domain for both the 34-hAdK and 55-hAdK complexes (comparison with the enzyme starting structure obtained after IFD, C-terminal domain excluded from the analysis), while the rotation angle was approximately 9° for the 1c-hAdK and 30-hAdK complexes. Notably, no dynamic domain was found for the 57-hAdK complex; thus, the enzyme persisted in its closed conformation throughout the simulation. The preference for an open enzyme conformation as well as the rotation angle of the small lid

domain during MD simulation of nucleoside inhibitors agreed with modeling studies reported by other authors.^{46,47}

To further support our hypothesis, we subjected 1a to the same computational protocol (IFD followed by 30 ns of MD simulation run in triplicate, see Supporting Information, Table S1). The obtained docking pose (Supporting Information, Figure S5A) superimposed well with the experimental binding mode for 1c (RMSD = 0.37 Å), and both the purine core and C2' and C3' hydroxyl groups featured the same interaction pattern observed for the methanocarpa derivatives. Additional H-bond interactions were detected for the side chains of Gln38 and Asp300 with the ribose ether oxygen and the C5' hydroxyl group, respectively. The analysis of the trajectory (Supporting Information, Video S4) was consistent with the conformational analysis of the 1c-hAK complex: in particular, 1a persisted for most of the simulation time in the C1'-*exo* and C2'-*endo* (S) conformations (65% and 25% of the trajectory, respectively) and maintained a stable network of interactions, such as the bidentate H-bond with the side chain of Asp18, H-bonds to the backbone of Gly64, Ser65, and the side chain of Asn14, and the π - π stacking interaction with Phe170. Concerning the enzyme conformation, superimposition of MD average protein structure with the enzyme in the closed conformation (magenta and gray ribbons in Supporting Information, Figure S5B, respectively) revealed that the enzyme persisted in the closed conformation. Similarly to what was observed for the 57-hAdK complex, no dynamic domain was found for the 1a-hAK complex.

DISCUSSION

The application of AdK inhibitors to CNS disorders such as epilepsy and chronic pain experienced a hiatus during the past decade, due to possible side effects of the known inhibitors. Critical gaps to be addressed are isoform selectivity (cytoplasmic versus nuclear AdK), cell-type selectivity (neuron versus astrocyte), and trans-membrane transport. Thus, there is a need for a new class of inhibitors with enhanced selectivities, such as nucleosides that have a major distinction from the known riboside inhibitors such as 1a and 2.

We have utilized an alternative ribose-like ring system, e.g., two isomeric methanocarpa pseudoribose substitutions, in nucleoside derivatives to demonstrate that inhibition of AdK is compatible with these major structural changes. By virtue of the bridged bicycloaliphatic ring, a rigid (S) 3'-*exo* or (N) 2'-*exo* envelope conformation is permanently locked in these nucleoside analogues. The most potent inhibitors, (S)-methanocarpa derivatives 34, 38a, 38b, and 38c and (N)-methanocarpa derivative 55 were approximately 2-fold less potent than the reference compound 2. The apparent discrepancy for the IC₅₀ of 2 in our study of 48 nM, compared to its previously reported sub-nM IC₅₀,²² is because of the use of a different assay system. The previous assay used was based on a radioactive assay using adenosine as a substrate,¹⁷ and ours is a commercial spectrophotometric assay based on inosine as substrate.

The presence of a p-F substitution in either the 5-phenyl 38b or 4-phenylamino 38c ring in the (S)-methanocarpa series maintained the inhibitory potency of analogue 38a. We synthesized and compared potencies of two pairs of corresponding (S) and (N)-methanocarpa 4'-CH₂OH derivatives. We conclude that both conformations maintain potency at hAdK and can provide a path to novel nucleoside inhibitors. 5-Iodo analogues 32 (S) and 57 (N) displayed comparable potency, and the pair of more potent 4-phenylamino-5-phenyl

analogues **34** (S) and **55** (N) also displayed similar IC₅₀ values. This conclusion was consistent with X-ray structures of known inhibitors bound to hAdK^{36,37} and with molecular docking and MD analyses of several of the present derivatives.

A similar attempt to constrain analogues of 2'-deoxynucleoside inhibitors of adenosine deaminase (ADA) using the [3.1.0]bicyclohexane ring system failed.⁴⁸ Although the enzyme preferred the (N) methanocarba nucleoside over the (S), the relative rate of deamination was ~100-fold lower than adenosine, which suggested a possible role of the 4'-oxygen atom of native ribose in an anomeric effect to assist hydrolysis by ADA. In (S)-methanocarba nucleosides, the *syn*-conformation of the pseudoglycosidic bond is thought to be more stable than the *anti*-conformation, but in the X-ray structure of hAdK complexes, the nucleoside *anti*-conformation is present. The analysis of MD simulation starting from the X-ray complex suggests that the *anti* conformation best suits the electrostatic potential distribution of the enzyme active site, featuring a highly hydrophobic cavity that hosts the purine core next to a region full of charged residues that anchors the ribose ring.

As far as the conformational preference of the enzyme is concerned, the active site of AdK appears to be highly flexible, as both (S)-methanocarba (C3'-*exo*, $P = 198^\circ$) compound **34** and its (N)-methanocarba (C2'-*exo*, $P = 342^\circ$) analogue **55** are equipotent inhibitors. It has to be noted that the synthesized locked conformers deviate by $\pm 18^\circ$ from the (N) and (S) ideal (N) and (S) conformations of ribose.^{32,35} Interestingly, the near equipotency of (N) and (S) methanocarba isomers did not apply to conformationally locked analogues of **1a** lacking the phenyl moieties. (S)-Conformers **30** and **49** were weak inhibitors of hAdK, while the inhibitory potencies of **1a** and its (N)-methanocarba counterpart **57** were comparable. A possible explanation is provided by the modeling results: the bulky N⁶,C7-diphenyl substituents do not fit into the hAdK closed form and, as emerged from MD simulations, induced the opening of the small lid domain. The enzyme open conformation is expected to exhibit a higher plasticity with respect to closed conformation to which smaller **1a** mimics are predicted to bind. As a consequence, this enzyme conformation could accommodate the pseudosugar ring locked in either the (S) or (N) conformation. Thus, hAdK might indeed prefer the (N)-conformer as inhibitor in the closed/catalytic-phase of the enzyme.

When comparing pairs of methanocarba isomers, a distinction needs to be made between those having or lacking bulky phenyl groups, which largely determine the enzyme conformational preference. Indeed, when phenyl groups are attached to the purine core, the opening of the small lid domain occurs to host them. Those groups establish additional van der Waals interactions and hydrophobic contacts with the lid, which compensate for any geometrical factors in the ribose region. However, for the small nucleoside inhibitors, the conformation of the pseudoribose ring predominates. In compound **30**, the interactions with the backbone NH groups of Gly64 and Ser65 appear to be missing because of steric hindrance of the cyclopropyl ring of the (S) isomer. Those interactions impose a specific conformation of adenosine analogues and might help maintain the enzyme in the closed conformation by allowing the C2' and C3' hydroxyl groups of the inhibitors to H-bond with Asp18 of the lid. A mutagenesis study of AdK from *Leishmania donovani* reported the indispensable role of Asp16 (the equivalent of Asp18 in the hAdK) for the catalytic activity and suggested its involvement

in a bidentate interaction with the hydroxyl group in C2' and C3' position of adenosine.⁸⁰

Thus, we have discovered novel high potency inhibitors of hAdK, which can now be evaluated in vivo, for example, in effects on DNA methylation, in comparison to riboside inhibitors such as **1a**.⁵ The brain penetration by these analogues remains undetermined, which could be a complicating factor because nucleosides often have low entry into the CNS.⁴⁹ Nevertheless, the slightly greater hydrophobicity of the (S)-methanocarba derivatives (cLogP of **49** is -0.11 ; tPSA is 120 Å) compared to ribosides (cLogP of the tetrahydrofuryl equivalent of **49** is -1.15 ; tPSA is 130 Å) might be beneficial for crossing the blood–brain barrier. Furthermore, there remains the possibility that the specificity for AdK is enhanced in these (S)-methanocarba derivatives, which is crucial for avoiding possible side effects already noted for known AdK inhibitors. Although we have shown the feasibility of using this ribose conformational constraint in AdK inhibitors, there remains room for structural optimization to improve the inhibitory potency, considering that some of the known inhibitors achieve sub-nM affinity.

The interaction of these (S)-methanocarba analogues with nucleoside transporters that are relevant to adenosine derivatives, such as ENT1 and CNT2,⁵⁰ remains to be characterized. The ability to serve as substrate or inhibitor of nucleoside transporters could affect the biodistribution or availability of the compounds in vivo.^{49,51} An analogue of the potent ENT1 inhibitor S-(4-nitrobenzyl)-thioinosine containing the opposite ring twist conformation ((N) methanocarba) was shown to inhibit ENT1, and other fixed conformations of 2'-deoxynucleosides were evaluated.^{52,53} (S)-Methanocarba 2'-deoxyadenosine inhibited both ENTs and CNTs, although less potently than 2'-deoxyadenosine.

The bioavailability and the in vivo activity of these inhibitors remain to be determined. Other nucleoside derivatives were protective in seizure models when administered peripherally.¹⁷ For example, the Br analogue of carbocyclic nucleoside **2** was found to be orally active in vivo in models of pain and inflammation.²¹ 5'-Deoxynucleoside analogues of **1a** were noted to be more potent in vivo than 5'-amino analogues, possibly because of enhanced passage across the blood–brain barrier by virtue of being less polar.¹⁷ Among the new (S)-methanocarba AdK inhibitors, 5'-deoxy analogue **38a** and especially the fluoro analogues **38b** and **38c** appear to be the least polar based on their tendency to dissolve in organic solvents.

It is possible that transient treatment with AdK inhibitors would have long-lasting therapeutic benefits for treatment of CNS disorders, not only by raising the basal level of AR activation but also through epigenetic reprogramming. A high level of adenosine in the brain drives the enzymatic equilibrium in the presence of S-adenosylhomocysteine (SAH) hydrolase in the direction of increased SAH formation. SAH in turn inhibits DNA methyltransferases through product inhibition.^{39,54} Because the epigenetic effects related to changes in the DNA methylation status would persist, it might be possible to reduce the duration of drug administration, thus avoiding toxicities associated with prolonged, chronic dosing. A transient dosing regimen might also avoid possible side effects such as liver toxicity.¹² Compounds **38a** and **55** were submitted to the Psychoactive Drug Screening Program (PDSP) for screening at 45 receptors, channels, and transporters (Supporting Information).⁵⁵ **38a** was found to inhibit radioligand binding at the

human 5HT₇ (serotonin) receptor with a K_i value of 0.71 μM and did not substantially inhibit binding at any of the other off-target sites examined (<50% inhibition at 10 μM). **55** was found to inhibit radioligand binding at the human 5HT_{2B} receptor with a K_i value of 51 nM and did not substantially inhibit binding at any of the other off-target sites examined. Also, **38a** was found to be inactive (10 μM) as agonist or antagonist at human P2Y₁, P2Y₂, P2Y₄, and P2Y₁₁Rs (calcium transients) expressed in 1321N1 astrocytoma cells and protease-activated receptor (PAR)1 expressed in mouse KOLF cells. Nevertheless, the off-target interactions of the present set of compounds would have to be examined more extensively.

CONCLUSION

In conclusion, the development of novel AdK inhibitors, by virtue of their ability to raise the level of endogenous adenosine, particularly in disease states, remains of interest for the potential treatment of seizures and neurodegenerative and inflammatory conditions. We demonstrated that the class of constrained bicyclic ribonucleoside analogues retain inhibitory activity at this enzyme and are amenable to structural modification to enhance the potency. The SAR for ring-constrained analogues deviates the SAR determined previously for ribosides; analogues with aryl groups at the 7-deaza and N⁶ positions of adenine are greatly favored, with (S) \approx (N). We determined that the (S) conformation permits a range of substitutions, but amino derivatives **45** and **49** were much less potent than expected from the ribose equivalents. However, a difference between the (N)- and (S)-methanocarba series is that the methanocarba equivalent of reference riboside **1a** is more potent in the (N) than in the (S) series (**55** and **30**, respectively). We have identified compounds **34**, **38a**, **38b**, **38c**, and **55** as hAdK inhibitors with IC₅₀ values of \sim 100 nM. The successful docking and MD simulation of selected members of this series in the enzyme structure suggests that a structure-based design approach for further enhancement is possible. Although we have not yet explored all of the potential off-target effects and adenosine-receptor related side effects of this structural class, it is possible that the novel nonribose ring system will provide a cleaner pharmacological profile. The potent AdK inhibitors in this study are now ready for further tests in animal models of epilepsy and its development.

EXPERIMENTAL SECTION

Chemical Synthesis. Materials and Methods. All chemicals and anhydrous solvents were obtained directly from commercial sources. All reactions were carried out under nitrogen atmosphere using anhydrous solvents unless specified otherwise. Room temperature or rt refers to 25 \pm 5 $^\circ\text{C}$. Silica-gel precoated with F254 on aluminum plates were used for TLC. The spots were examined under ultraviolet light at 254 nm and further visualized by anisaldehyde or cerium ammonium molybdate stain solution. Column chromatography was performed on silica gel (40–63 μm , 60 \AA). NMR spectra were recorded on a Bruker 400 MHz spectrometer. Chemical shifts are given in ppm (δ), calibrated to the residual solvent signals or TMS. High resolution mass (HRMS) measurements were performed on a proteomics optimized Q-TOF-2 (Micromass-Waters). The RP-HPLC was performed using Phenomenex Luna 5 μm C18(2)100A, AXIA, 21.2 mm \times 250 mm column. Purity was determined using Agilent ZORBAX SB-Aq, 5 μm , 4.6 mm \times 150 mm column attached to Agilent 1100 HPLC system and a linear gradient of acetonitrile/water as mobile phase with a flow rate of 1.0 mL/min (acetonitrile/5 mM tetrabutylammonium dihydrogen phosphate in the case of **45** and **49**). The purity of all

screened compounds is >95% as determined by HPLC with detection at 254 nm. tPSA and cLogP were calculated using ChemDraw Professional version 15.0 (PerkinElmer, Boston, MA). All chemical reagents were obtained from Sigma-Aldrich (St. Louis, MO), except 2-(4,6-dichloropyrimidin-5-yl)acetaldehyde **25** (Small Molecules, Inc., Hoboken, NJ).

7-((3aS,3bS,4aS,5R,5aR)-5-(((tert-Butyldiphenylsilyloxy)methyl)-2,2-dimethyltetrahydrocyclopropa[3,4]cyclopenta[1,2-d][1,3]-dioxol-3b(3aH)-yl)-4-chloro-7H-pyrrolo[2,3-d]pyrimidine (**26**). The amine **24** (200 mg, 0.46 mmol) was dissolved in ethanol (4 mL). To this was added 4,6-dichloropyrimidin-5-acetaldehyde **25** (88 mg, 0.46 mmol) and triethylamine (TEA, 128 μL , 0.92 mmol). The reaction mixture was heated to 90 $^\circ\text{C}$ under reflux condenser overnight, volatiles evaporated under reduced pressure, and residue purified by silica gel flash column chromatography to afford compound **26** as a white foam (200 mg, 76%, R_f = 0.45, TLC eluent = 20% ethyl acetate in hexanes). ¹H NMR (400 MHz, CDCl₃) δ 8.40 (s, 1H), 7.79–7.65 (m, 4H), 7.49–7.34 (m, 6H), 7.28 (d, J = 3.6 Hz, 1H), 6.51 (d, J = 3.6 Hz, 1H), 4.98 (dd, J = 1.6, 7.1 Hz, 1H), 4.60 (dd, J = 0.8, 7.1 Hz, 1H), 4.12 (d, J = 7.9 Hz, 2H), 2.58 (t, J = 7.9 Hz, 1H), 2.11 (ddd, J = 1.4, 5.5, 9.9 Hz, 1H), 1.62 (t, J = 5.6 Hz, 1H), 1.58 (s, 3H), 1.44 (ddd, J = 1.8, 5.8, 9.8 Hz, 1H), 1.22 (s, 3H), 1.08 (s, 9H). ¹³C NMR (101 MHz, CDCl₃) δ 151.72, 151.64, 150.44, 135.63, 135.61, 133.56, 133.50, 130.37, 129.81, 129.79, 127.75, 118.19, 111.51, 99.44, 84.57, 83.24, 65.03, 49.68, 47.51, 31.32, 26.90, 26.36, 24.06, 19.34, 16.63. HRMS m/z [M + H]⁺ for C₃₂H₃₆ClN₃O₃Si calculated 574.2293, found 574.2290.

7-((3aS,3bS,4aS,5R,5aR)-5-(((tert-Butyldiphenylsilyloxy)methyl)-2,2-dimethyltetrahydrocyclopropa[3,4]cyclopenta[1,2-d][1,3]-dioxol-3b(3aH)-yl)-4-chloro-5-iodo-7H-pyrrolo[2,3-d]pyrimidine (**27**). To a dried mixture of compound **26** (200 mg, 0.35 mmol) and *N*-iodosuccinimide (NIS, 135 mg, 0.42 mmol) was added anhydrous DMF (5 mL) under nitrogen atmosphere. The solution was heated to 65 $^\circ\text{C}$ with stirring for 6 h. The volatiles were evaporated under vacuum, and the residue was purified by silica gel flash column chromatography to afford **27** as a white foam (225 mg, 92%, R_f = 0.50, TLC eluent = 20% ethyl acetate in hexanes). ¹H NMR (400 MHz, CDCl₃) δ 8.36 (s, 1H), 7.80–7.68 (m, 4H), 7.53–7.34 (m, 7H), 4.94 (d, J = 7.0 Hz, 1H), 4.59 (d, J = 7.0 Hz, 1H), 4.08 (d, J = 7.9 Hz, 2H), 2.57 (t, J = 7.8 Hz, 1H), 2.10 (dd, J = 5.5, 9.9 Hz, 1H), 1.61 (t, J = 5.6 Hz, 1H), 1.57 (s, 3H), 1.42 (dd, J = 5.8, 10.0 Hz, 1H), 1.21 (s, 3H), 1.08 (s, 9H). ¹³C NMR (101 MHz, CDCl₃) δ 152.47, 151.39, 150.77, 135.62, 135.60, 135.58, 134.79, 133.47, 133.44, 129.84, 129.82, 129.64, 127.77, 127.77, 127.71, 117.52, 111.61, 84.40, 83.14, 64.92, 49.87, 47.43, 31.38, 26.89, 26.56, 26.34, 24.04, 19.33, 16.64. HRMS m/z [M + H]⁺ for C₃₂H₃₅ClIN₃O₃Si calculated 700.1259, found 700.1253.

(1*R*,2*S*,3*R*,4*R*,5*S*)-1-(4-Chloro-5-iodo-7H-pyrrolo[2,3-d]pyrimidin-7-yl)-4-(hydroxymethyl)bicyclo[3.1.0]hexane-2,3-diol (**28**). To compound **27** (20 mg, 0.029 mmol) was added 70% aqueous trifluoroacetic acid (TFA, 1.5 mL) and the mixture stirred at room temperature for 1.5 h. The volatiles were evaporated under vacuum, and the residual TFA was chased first with water (2 \times 2 mL) and then neutralized with a mixture of water (2 mL) and a few drops of triethylamine. The residue after evaporation was purified by silica gel flash column chromatography to afford **28** as a white solid (10 mg, 83%, R_f = 0.50, TLC eluent = 10% methanol in dichloromethane). ¹H NMR (400 MHz, CD₃OD) δ 8.63 (s, 1H), 7.86 (s, 1H), 4.69 (dd, J = 2.0, 6.5 Hz, 1H), 4.14–4.02 (m, 2H), 3.93 (dd, J = 4.9, 11.3 Hz, 1H), 2.34 (t, J = 4.6 Hz, 1H), 2.01–1.92 (m, 2H), 1.31 (ddd, J = 2.0, 4.3, 8.2 Hz, 1H). ¹³C NMR (101 MHz, CD₃OD) δ 153.63, 152.31, 151.19, 139.06, 119.11, 77.64, 73.84, 65.49, 51.54, 51.31, 50.55, 26.50, 15.48. HRMS m/z [M + H]⁺ for C₁₃H₁₃ClIN₃O₃ calculated 421.9768, found 421.9771.

7-((3aS,3bR,4aS,5R,5aR)-5-(((tert-Butyldiphenylsilyloxy)methyl)-2,2-dimethyltetrahydrocyclopropa[3,4]cyclopenta[1,2-d][1,3]-dioxol-3b(3aH)-yl)-5-iodo-7H-pyrrolo[2,3-d]pyrimidin-4-amine (**29**). Compound **27** (75 mg, 0.11 mmol) was placed in a glass pressure tube with stir bar and treated with ethanol (5 mL) followed by 7 N ammonia in methanol (5 mL). The tube was capped tightly and heated to 120 $^\circ\text{C}$ for 18 h with stirring. The solvents were evaporated and the residue purified by silica gel flash column chromatography to afford **29** as a white solid (65 mg, 89%, R_f = 0.45, TLC eluent = 5% methanol in

dichloromethane). ^1H NMR (400 MHz, CDCl_3) δ 7.82 (s, 1H), 7.75–7.65 (m, 3H), 7.51–7.44 (m, 2H), 7.43–7.36 (m, 5H), 7.31 (s, 1H), 4.90 (dd, $J = 1.6, 7.1$ Hz, 1H), 4.58 (dd, $J = 1.3, 7.2$ Hz, 1H), 4.00 (d, $J = 7.6$ Hz, 1H), 2.56 (t, $J = 7.5$ Hz, 1H), 2.12 (ddd, $J = 1.4, 5.4, 9.9$ Hz, 1H), 1.62 (t, $J = 5.7$ Hz, 1H), 1.57 (s, 3H), 1.40 (ddd, $J = 1.8, 5.9, 10.0$ Hz, 1H), 1.22 (s, 4H), 1.08 (s, 9H). ^{13}C NMR (101 MHz, CDCl_3) δ 152.60, 148.78, 141.90, 135.61, 135.55, 133.35, 133.24, 132.89, 130.02, 129.94, 127.84, 127.80, 111.83, 103.11, 84.65, 83.15, 64.89, 50.27, 47.28, 31.53, 26.91, 26.86, 26.32, 24.04, 19.33, 16.72. HRMS m/z [$\text{M} + \text{H}$] $^+$ for $\text{C}_{32}\text{H}_{37}\text{IN}_4\text{O}_3\text{Si}$ calculated 681.1758, found 681.1749.

(1*R*,2*S*,3*R*,4*R*,5*S*)-1-(4-Amino-5-iodo-7*H*-pyrrolo[2,3-*d*]pyrimidin-7-yl)-4-(hydroxymethyl)bicyclo[3.1.0]hexane-2,3-diol (**30**). Following the procedure described to synthesize **28**, compound **29** (13 mg, 0.019 mmol) afforded **30** as a white solid which was further purified by RP-HPLC (3.6 mg, 47%, $R_f = 0.25$, TLC eluent = 10% methanol in dichloromethane; RP-HPLC (C18) $R_t = 18.9$ min, water/acetonitrile 75/25 \rightarrow 25/75 in 40 min at 5 mL/min). ^1H NMR (400 MHz, CD_3OD) δ 8.08 (s, 1H), 7.35 (s, 1H), 4.57 (dd, $J = 2.0, 6.6$ Hz, 1H), 4.05–3.97 (m, 2H), 3.79 (dd, $J = 3.6, 11.5$ Hz, 1H), 2.25 (t, $J = 2.9$ Hz, 1H), 1.84–1.76 (m, 2H), 1.18–1.09 (m, 1H). ^{13}C NMR (101 MHz, CD_3CN) δ 158.58, 152.56, 150.84, 132.31, 105.11, 77.55, 74.12, 65.56, 51.15, 50.56, 49.18, 26.79, 14.94. HRMS m/z [$\text{M} + \text{H}$] $^+$ for $\text{C}_{13}\text{H}_{15}\text{IN}_4\text{O}_3$ calculated 403.0267, found 403.0269.

7-((3*aS*,3*bR*,4*aS*,5*R*,5*aR*)-5-(((*tert*-Butyldiphenylsilyloxy)methyl)-2,2-dimethyltetrahydrocyclopropa[3,4]cyclopenta[1,2-*d*][1,3]-dioxol-3*b*(3*aH*)-yl)-*N*-4-fluorophenyl)-5-phenyl-7*H*-pyrrolo[2,3-*d*]pyrimidin-4-amine (**31a**). To a solution of predried compound **27** (75 mg, 0.11 mmol) and aniline (12 μL , 0.13 mmol) in anhydrous THF (1 mL) at -20°C under nitrogen atmosphere was added potassium *t*-butoxide solution (1 M in THF, 160 μL , 0.16 mmol) dropwise and stirred at this temperature for 1 h. The reaction was quenched by adding satd NH_4Cl (1 mL) and the products extracted into ethyl acetate (3 \times 2 mL). The separated organic layers were combined, washed with brine, dried over anhydrous Na_2SO_4 , and evaporated, and the residue was purified by silica gel flash column chromatography to afford **31a** as a white foam (65 mg, 80%, $R_f = 0.30$, TLC eluent = 10% ethyl acetate in hexanes). ^1H NMR (400 MHz, CDCl_3) δ 8.27 (s, 1H), 8.23 (brs, 1H), 7.78–7.64 (m, 8H), 7.50–7.34 (m, 7H), 7.21 (s, 1H), 4.99 (dd, $J = 1.6, 7.1$ Hz, 1H), 4.59 (dd, $J = 1.1, 7.0$ Hz, 1H), 4.11 (d, $J = 7.8$ Hz, 2H), 2.55 (t, $J = 7.8$ Hz, 1H), 2.08 (ddd, $J = 1.3, 5.4, 9.8$ Hz, 1H), 1.63–1.54 (m, 4H), 1.46–1.38 (m, 1H), 1.22 (s, 3H), 1.09 (s, 9H). HRMS m/z [$\text{M} + \text{H}$] $^+$ for $\text{C}_{38}\text{H}_{41}\text{IN}_4\text{O}_3\text{Si}$ calculated 757.2071, found 757.2067.

7-((3*aS*,3*bR*,4*aS*,5*R*,5*aR*)-5-(((*tert*-Butyldiphenylsilyloxy)methyl)-2,2-dimethyltetrahydrocyclopropa[3,4]cyclopenta[1,2-*d*][1,3]-dioxol-3*b*(3*aH*)-yl)-*N*-(4-fluorophenyl)-5-iodo-7*H*-pyrrolo[2,3-*d*]pyrimidin-4-amine (**31b**). Following the procedure described for the synthesis of **31a**, compound **27** (60 mg, 0.086 mmol) gave **31b** as a white foam (47 mg, 70%, $R_f = 0.2$, TLC eluent = 10% ethyl acetate in hexanes). ^1H NMR (400 MHz, CDCl_3) δ 8.23 (s, 1H), 7.89 (s, 1H), 7.77–7.64 (m, 6H), 7.48–7.35 (m, 6H), 7.17 (s, 1H), 7.09 (dd, $J = 8.3, 9.0$ Hz, 2H), 5.01 (dd, $J = 1.6, 7.1$ Hz, 1H), 4.62–4.56 (m, 1H), 4.13 (d, $J = 8.0$ Hz, 2H), 2.54 (t, $J = 8.0$ Hz, 1H), 2.07 (ddd, $J = 1.3, 5.4, 9.8$ Hz, 1H), 1.57 (s, 3H), 1.55 (m, 1H), 1.41 (ddd, $J = 1.7, 5.6, 9.8$ Hz, 1H), 1.21 (s, 3H), 1.08 (s, 9H). ^{19}F NMR (376 MHz, CDCl_3) δ -119.03 . HRMS m/z [$\text{M} + \text{H}$] $^+$ for $\text{C}_{38}\text{H}_{40}\text{FIN}_4\text{O}_3\text{Si}$ calculated 775.1977, found 775.1971.

(1*R*,2*S*,3*R*,4*R*,5*S*)-4-(Hydroxymethyl)-1-(5-iodo-4-(phenylamino)-7*H*-pyrrolo[2,3-*d*]pyrimidin-7-yl)bicyclo[3.1.0]hexane-2,3-diol (**32**). Following the reaction procedure described for the synthesis of **28**, compound **31a** (20 mg, 0.035 mmol) gave **32** as a white solid which was further purified by RP-HPLC (3.35 mg, 27%, $R_f = 0.45$, TLC eluent = 10% methanol in dichloromethane; RP-HPLC (C18) $R_t = 25.6$ min, water/acetonitrile 50/50 \rightarrow 10/90 in 40 min at 5 mL/min). ^1H NMR (400 MHz, CD_3OD) δ 8.27 (s, 1H), 7.74 (dd, $J = 1.1, 8.7$ Hz, 1H), 7.45 (s, 1H), 7.41–7.33 (m, 2H), 7.17–7.09 (m, 1H), 4.60 (dd, $J = 2.0, 6.6$ Hz, 1H), 4.08–3.99 (m, 2H), 3.81 (dd, $J = 3.7, 11.5$ Hz, 1H), 2.29–2.25 (m, 1H), 1.87–1.79 (m, 2H), 1.17 (ddp, $J = 2.1, 3.6, 5.7$ Hz, 1H). HRMS m/z [$\text{M} + \text{H}$] $^+$ for $\text{C}_{19}\text{H}_{19}\text{IN}_4\text{O}_3$ calculated 479.0580, found 479.0589.

7-((3*aS*,3*bR*,4*aS*,5*R*,5*aR*)-5-(((*tert*-Butyldiphenylsilyloxy)methyl)-2,2-dimethyltetrahydrocyclopropa[3,4]cyclopenta[1,2-*d*][1,3]-dioxol-3*b*(3*aH*)-yl)-*N*,5-diphenyl-7*H*-pyrrolo[2,3-*d*]pyrimidin-4-amine (**33a**). A mixture of DME (1.7 mL) and ethanol (0.3 mL) was heated to 90°C for 10 min and cooled to room temperature. This solution was added to a vacuum-dried mixture of **31a** (75 mg, 0.13 mmol), phenylboronic acid (19 mg, 0.16 mmol), and $\text{Pd}(\text{PPh}_3)_4$ (7.5 mg, 0.007 mmol). A sonicated aqueous saturated Na_2CO_3 solution was added to this mixture, and the flask immersed in to a preheated oil bath at 90°C and stirred for 7 h. The solvents were evaporated under vacuum, and the residue was partitioned between water and dichloromethane (3 \times 10 mL), the organic layer separated, dried over anhydrous Na_2SO_4 , and then evaporated. The residue was purified by silica gel flash column chromatography to afford pure product **33a** as a white foam (60 mg, 86%, $R_f = 0.25$, TLC eluent = 10% ethyl acetate in hexanes). ^1H NMR (400 MHz, CDCl_3) δ 8.32 (s, 1H), 7.80–7.66 (m, 6H), 7.52–7.33 (m, 11H), 7.31–7.26 (m, 2H), 7.07 (s, 1H), 7.05–6.99 (m, 1H), 5.13 (dd, $J = 1.5, 7.1$ Hz, 1H), 4.64 (d, $J = 7.0$ Hz, 1H), 4.18 (d, $J = 7.9$ Hz, 2H), 2.58 (t, $J = 7.9$ Hz, 1H), 2.14 (ddd, $J = 1.3, 5.5, 9.8$ Hz, 1H), 1.64–1.56 (m, 4H), 1.49 (ddd, $J = 1.7, 5.7, 9.8$ Hz, 1H), 1.24 (s, 3H), 1.10 (s, 9H). HRMS m/z [$\text{M} + \text{H}$] $^+$ for $\text{C}_{44}\text{H}_{46}\text{N}_4\text{O}_3\text{Si}$ calculated 707.3417, found 707.3405.

7-((3*aS*,3*bR*,4*aS*,5*R*,5*aR*)-5-(((*tert*-Butyldiphenylsilyloxy)methyl)-2,2-dimethyltetrahydrocyclopropa[3,4]cyclopenta[1,2-*d*][1,3]-dioxol-3*b*(3*aH*)-yl)-*N*-(4-fluorophenyl)-5-phenyl-7*H*-pyrrolo[2,3-*d*]pyrimidin-4-amine (**33b**). Following the procedure described for the synthesis of **33a**, compound **31b** (50 mg, 0.0645 mmol) gave **33b** as a white foam (35 mg, 75%, $R_f = 0.15$, TLC eluent = 10% ethyl acetate in hexanes). ^1H NMR (400 MHz, CDCl_3) δ 8.25 (s, 1H), 7.73 (ddt, $J = 1.7, 4.0, 8.1$ Hz, 5H), 7.56–7.29 (m, 13H), 7.07 (s, 1H), 7.03–6.81 (m, 2H), 5.11 (dd, $J = 1.6, 7.1$ Hz, 1H), 4.69–4.57 (m, 1H), 4.16 (d, $J = 7.9$ Hz, 2H), 2.58 (t, $J = 7.8$ Hz, 1H), 2.14 (ddd, $J = 1.3, 5.4, 9.9$ Hz, 1H), 1.61 (t, $J = 6.0$ Hz, 1H), 1.58 (s, 3H), 1.49 (ddd, $J = 1.8, 5.8, 9.8$ Hz, 1H), 1.24 (s, 3H), 1.09 (s, 9H). ^{19}F NMR (376 MHz, CDCl_3) δ -119.7 . HRMS m/z [$\text{M} + \text{H}$] $^+$ for $\text{C}_{44}\text{H}_{45}\text{FN}_4\text{O}_3\text{Si}$ calculated 725.3323, found 725.3322.

7-((3*aS*,3*bR*,4*aS*,5*R*,5*aR*)-5-(((*tert*-Butyldiphenylsilyloxy)methyl)-2,2-dimethyltetrahydrocyclopropa[3,4]cyclopenta[1,2-*d*][1,3]-dioxol-3*b*(3*aH*)-yl)-5-(4-fluorophenyl)-*N*-phenyl-7*H*-pyrrolo[2,3-*d*]pyrimidin-4-amine (**33c**). Following the procedure described for the synthesis of **33a**, compound **31a** (50 mg, 0.0645 mmol) gave **33c** as a white foam (40 mg, 75%, $R_f = 0.15$, TLC eluent = 10% ethyl acetate in hexanes). ^1H NMR (400 MHz, CDCl_3) δ 8.31 (s, 1H), 7.78–7.70 (m, 4H), 7.42 (ddd, $J = 2.0, 6.0, 8.3, 14.5$ Hz, 10H), 7.28 (t, $J = 7.8$ Hz, 3H), 7.15 (d, $J = 8.4$ Hz, 2H), 7.07–7.00 (m, 2H), 5.12 (dd, $J = 1.5, 7.1$ Hz, 1H), 4.64 (dd, $J = 1.3, 7.2$ Hz, 1H), 4.19 (d, $J = 7.9$ Hz, 2H), 2.58 (t, $J = 7.8$ Hz, 1H), 2.14 (ddd, $J = 1.3, 5.4, 9.8$ Hz, 1H), 1.61 (t, $J = 3.8$ Hz, 1H), 1.59 (s, 3H), 1.49 (ddd, $J = 1.7, 5.7, 9.8$ Hz, 1H), 1.24 (s, 3H), 1.10 (s, 9H). ^{19}F NMR (376 MHz, CDCl_3) δ -114.31 (q, $J = 3.7, 4.4$ Hz). HRMS m/z [$\text{M} + \text{H}$] $^+$ for $\text{C}_{44}\text{H}_{45}\text{FN}_4\text{O}_3\text{Si}$ calculated 725.3323, found 725.3317.

(1*R*,2*S*,3*R*,4*R*,5*S*)-4-(Hydroxymethyl)-1-(5-phenyl-4-(phenylamino)-7*H*-pyrrolo[2,3-*d*]pyrimidin-7-yl)bicyclo[3.1.0]hexane-2,3-diol (**34**). Following the reaction procedure described for the synthesis of **28**, compound **33a** (17 mg, 0.024 mmol) gave **34** as a white solid which was further purified by RP-HPLC (4.7 mg, 46%, $R_f = 0.25$, TLC eluent = 5% methanol in dichloromethane; RP-HPLC (C18) $R_t = 29.8$ min, water/acetonitrile 50/50 \rightarrow 10/90 in 40 min at 5 mL/min). ^1H NMR (400 MHz, CD_3OD) δ 8.32 (s, 1H), 7.65–7.51 (m, 4H), 7.51–7.42 (m, 3H), 7.33 (s, 1H), 7.30–7.22 (m, 2H), 7.03 (ddt, $J = 1.1, 7.1, 7.7$ Hz, 1H), 4.70 (dd, $J = 2.0, 6.6$ Hz, 1H), 4.14–4.01 (m, 2H), 3.81 (dd, $J = 3.6, 11.5$ Hz, 1H), 2.33–2.27 (m, 1H), 1.93–1.81 (m, 2H), 1.24 (ddd, $J = 2.1, 5.1, 8.9$ Hz, 1H). HRMS m/z [$\text{M} + \text{H}$] $^+$ for $\text{C}_{25}\text{H}_{24}\text{N}_4\text{O}_3$ calculated 429.1927, found 429.1935.

((3*aS*,3*bR*,4*aS*,5*R*,5*aR*)-2,2-Dimethyl-3*b*-(5-phenyl-4-(phenylamino)-7*H*-pyrrolo[2,3-*d*]pyrimidin-7-yl)hexahydrocyclopropa[3,4]-cyclopenta[1,2-*d*][1,3]dioxol-5-yl)methanol (**35a**). Compound **33a** (60 mg, 0.089 mmol) was dissolved in anhydrous THF (2 mL), treated with tetrabutylammonium fluoride (1 M in THF, 93 μL , 0.093 mmol) at 0°C , and stirred overnight at room temperature. The solvent was evaporated and the residue purified by silica gel flash

column chromatography to afford **35a** as a white foamy solid (38 mg, 96%, $R_f = 0.15$, TLC eluent = 30% ethyl acetate in hexanes). $^1\text{H NMR}$ (400 MHz, CDCl_3) δ 8.44 (s, 1H), 7.59–7.47 (m, 6H), 7.47–7.40 (m, 1H), 7.36–7.26 (m, 2H), 7.13 (s, 1H), 7.11–7.00 (m, 2H), 5.07 (dd, $J = 1.8, 6.9$ Hz, 1H), 4.90 (dd, $J = 1.6, 6.9$ Hz, 1H), 4.12 (d, $J = 11.5$ Hz, 1H), 3.89 (dt, $J = 3.14, 12.1$ Hz, 1H), 2.50 (dd, $J = 1.2, 3.2$ Hz, 1H), 2.10 (ddd, $J = 1.5, 5.2, 9.7$ Hz, 1H), 1.64–1.55 (m, 4H), 1.40–1.21 (m, 4H). HRMS m/z $[\text{M} + \text{H}]^+$ for $\text{C}_{28}\text{H}_{28}\text{N}_4\text{O}_3$ calculated 469.2240, found 469.2241.

((3*aS*,3*bR*,4*aS*,5*R*,5*aR*)-3*b*-(4-((4-Fluorophenyl)amino)-5-phenyl-7*H*-pyrrolo[2,3-*d*]pyrimidin-7-yl)-2,2-dimethylhexahydrocyclopropa[3,4]cyclopenta[1,2-*d*][1,3]dioxol-5-yl)methanol (**35b**). Following the procedure described for the synthesis of **35a**, compound **33b** (35 mg, 0.048 mmol) gave **35b** as a white foam (20 mg, 85%, $R_f = 0.35$, TLC eluent = 50% ethyl acetate in hexanes). $^1\text{H NMR}$ (400 MHz, CDCl_3) δ 8.53 (s, 1H), 7.51 (d, $J = 4.4$ Hz, 4H), 7.44 (ddd, $J = 2.5, 4.6, 9.0$ Hz, 3H), 7.14 (s, 1H), 6.99 (t, $J = 8.6$ Hz, 2H), 5.06 (dd, $J = 1.7, 6.9$ Hz, 1H), 4.89 (dd, $J = 1.5, 6.9$ Hz, 1H), 4.13 (dd, $J = 1.4, 11.4$ Hz, 1H), 3.93 (dd, $J = 3.1, 11.4$ Hz, 1H), 2.51 (dd, $J = 1.3, 3.0$ Hz, 1H), 2.10 (ddd, $J = 1.5, 5.2, 9.7$ Hz, 1H), 1.64–1.60 (m, 1H), 1.58 (s, 3H), 1.37–1.31 (m, 1H), 1.29 (s, 3H). $^{13}\text{C NMR}$ (101 MHz, CDCl_3) δ 160.33, 157.92, 154.57, 151.42, 150.10, 134.83, 134.80, 134.31, 129.39, 129.27, 128.04, 124.57, 122.33, 122.25, 116.28, 115.85, 115.63, 111.32, 102.48, 85.80, 84.72, 65.72, 50.36, 46.90, 32.12, 26.59, 24.41, 16.44. $^{19}\text{F NMR}$ (376 MHz, CDCl_3) δ –118.65. HRMS m/z $[\text{M} + \text{H}]^+$ for $\text{C}_{28}\text{H}_{27}\text{FN}_4\text{O}_3$ calculated 487.2145, found 487.2148.

((3*aS*,3*bR*,4*aS*,5*R*,5*aR*)-3*b*-(5-(4-Fluorophenyl)-(phenylamino)-7*H*-pyrrolo[2,3-*d*]pyrimidin-7-yl)-2,2-dimethylhexahydrocyclopropa[3,4]cyclopenta[1,2-*d*][1,3]dioxol-5-yl)methanol (**35c**). Following the procedure described for the synthesis of **35a**, compound **33c** (40 mg, 0.055 mmol) gave **35c** as a white foam (25 mg, 93%, $R_f = 0.15$, TLC eluent = 30% ethyl acetate in hexanes). $^1\text{H NMR}$ (400 MHz, CDCl_3) δ 8.51 (s, 1H), 7.49 (ddd, $J = 2.1, 3.2, 8.7$ Hz, 4H), 7.35–7.28 (m, 2H), 7.24–7.17 (m, 2H), 7.12 (s, 1H), 7.07 (tt, $J = 1.1, 7.1$ Hz, 1H), 5.05 (dd, $J = 1.7, 6.9$ Hz, 1H), 4.89 (dd, $J = 1.4, 6.9$ Hz, 1H), 4.12 (dd, $J = 1.4, 11.4$ Hz, 1H), 3.91 (dd, $J = 3.0, 11.4$ Hz, 1H), 2.10 (ddd, $J = 1.5, 5.1, 9.8$ Hz, 1H), 1.61 (t, $J = 5.3$ Hz, 1H), 1.58 (s, 3H), 1.35–1.30 (m, 1H), 1.29 (s, 3H). $^{13}\text{C NMR}$ (101 MHz, CDCl_3) δ 163.88, 161.41, 154.55, 151.55, 150.10, 138.73, 131.07, 130.99, 130.31, 130.27, 129.18, 124.65, 123.71, 120.41, 116.45, 116.24, 115.12, 111.33, 102.65, 85.79, 84.72, 65.71, 50.35, 46.90, 32.11, 26.59, 24.41, 16.44. $^{19}\text{F NMR}$ (376 MHz, CDCl_3) δ –113.56. HRMS m/z $[\text{M} + \text{H}]^+$ for $\text{C}_{28}\text{H}_{27}\text{FN}_4\text{O}_3$ calculated 487.2145, found 487.2146.

N,5-Diphenyl-7-((3*aS*,3*bR*,4*aS*,5*S*,5*aR*)-2,2,5-trimethyltetrahydrocyclopropa[3,4]-cyclopenta[1,2-*d*][1,3]dioxol-3*b*(3*aH*)-yl)-7*H*-pyrrolo[2,3-*d*]pyrimidin-4-amine (**37a**). To a solution of compound **35a** (10 mg, 0.022 mmol) and DMAP (8 mg, 0.065 mmol) in anhydrous acetonitrile (0.5 mL) was added *O*-p-tolylchlorothionoformate (**36**, 8 μL , 0.052 mmol) dropwise at room temperature. The mixture was stirred for 4 h, and then the volatile organics were evaporated under reduced pressure. The residue was suspended in ethyl acetate (5 mL) and washed with water and brine. The organic layer was dried over anhydrous sodium sulfate and the solvent evaporated to dryness. The residue obtained was dried under high vacuum for 2 h and then suspended in anhydrous toluene (1.5 mL). Tributyltin hydride (17 μL , 0.065 mmol) and azoisobutyronitrile (AIBN, 10 mg, 0.065 mmol) was added, and the flask was immersed in to an oil bath at 120 °C for 2 h. Volatile materials were evaporated, and the residue was purified by silica gel flash column chromatography to afford compound **37a** as a white foam (5 mg, 52%, $R_f = 0.60$, TLC eluent = 30% ethyl acetate in hexanes). $^1\text{H NMR}$ (400 MHz, CDCl_3) δ 8.49 (s, 1H), 7.58–7.46 (m, 6H), 7.46–7.38 (m, 1H), 7.33–7.26 (m, 2H), 7.05 (s, 1H), 7.04–6.99 (m, 1H), 6.94 (s, 1H), 5.31 (dd, $J = 1.7, 7.0$ Hz, 1H), 4.50 (dd, $J = 1.4, 7.0$ Hz, 1H), 2.40 (q, $J = 7.5$ Hz, 1H), 1.92 (ddd, $J = 1.4, 5.4, 9.7$ Hz, 1H), 1.56 (d, $J = 7.3$ Hz, 3H), 1.55 (s, 3H), 1.41 (ddd, $J = 1.8, 5.6, 9.7$ Hz, 1H), 1.27 (s, 3H). HRMS m/z $[\text{M} + \text{H}]^+$ for $\text{C}_{28}\text{H}_{28}\text{N}_4\text{O}_2$ calculated 453.2291, found 453.2285.

N-(4-Fluorophenyl)-5-phenyl-7-((3*aS*,3*bR*,4*aS*,5*S*,5*aR*)-2,2,5-trimethyltetrahydro-cyclopropa[3,4]cyclopenta[1,2-*d*][1,3]dioxol-3*b*

(3*aH*)-yl)-7*H*-pyrrolo[2,3-*d*]pyrimidin-4-amine (**37b**). Following the procedure described for the synthesis of **37a**, compound **35b** (20 mg, 0.041 mmol) gave **37b** as a white foam (5 mg, 57% based on 11 mg starting material recovered, $R_f = 0.75$, TLC eluent = 30% ethyl acetate in hexanes). $^1\text{H NMR}$ (400 MHz, CDCl_3) δ 8.45 (s, 1H), 7.58–7.29 (m, 8H), 7.08 (s, 1H), 6.99–6.86 (m, 2H), 5.28 (dd, $J = 1.6, 7.0$ Hz, 1H), 4.54–4.46 (m, 1H), 2.41 (q, $J = 7.5$ Hz, 1H), 1.93 (ddd, $J = 1.4, 5.4, 9.7$ Hz, 1H), 1.59–1.52 (m, 7H), 1.41 (ddd, $J = 1.9, 5.8, 9.8$ Hz, 1H), 1.27–1.26 (m, 3H). $^{19}\text{F NMR}$ (376 MHz, CDCl_3) δ –119.6. HRMS m/z $[\text{M} + \text{H}]^+$ for $\text{C}_{28}\text{H}_{27}\text{FN}_4\text{O}_2$ calculated 471.2188, found 471.2188.

5-(4-Fluorophenyl)-*N*-phenyl-7-((3*aS*,3*bR*,4*aS*,5*S*,5*aR*)-2,2,5-trimethyltetrahydro-cyclopropa[3,4]cyclopenta[1,2-*d*][1,3]dioxol-3*b*(3*aH*)-yl)-7*H*-pyrrolo[2,3-*d*]pyrimidin-4-amine (**37c**). Following the procedure described for the synthesis of **37a**, compound **35c** (25 mg, 0.051 mmol) gave **37c** as a white foam (7 mg, 90% based on 12 mg starting material recovered, $R_f = 0.75$, TLC eluent = 30% ethyl acetate in hexanes). $^1\text{H NMR}$ (400 MHz, CDCl_3) δ 8.47 (s, 1H), 7.39 (brs, 4H), 7.31–7.20 (m, 3H), 7.11 (t, $J = 7.8$ Hz, 2H), 7.05 (s, 1H), 7.05–7.00 (m, 1H), 5.28 (dd, $J = 1.7, 7.0$ Hz, 1H), 4.50 (dd, $J = 1.4, 7.1$ Hz, 1H), 2.41 (q, $J = 7.4$ Hz, 1H), 1.94 (ddd, $J = 1.5, 5.4, 9.7$ Hz, 1H), 1.59–1.52 (m, 7H), 1.43–1.37 (m, 1H), 1.27 (s, 3H). $^{19}\text{F NMR}$ (376 MHz, CDCl_3) δ –114.30. HRMS m/z $[\text{M} + \text{H}]^+$ for $\text{C}_{28}\text{H}_{27}\text{FN}_4\text{O}_2$ calculated 471.2196, found 471.2204.

(1*R*,2*S*,3*R*,4*S*,5*S*)-4-Methyl-1-(5-phenyl-4-(phenylamino)-7*H*-pyrrolo[2,3-*d*]pyrimidin-7-yl)bicyclo[3.1.0]hexane-2,3-diol (**38a**). Following the reaction procedure described for the synthesis of **28**, compound **37** (5 mg, 0.011 mmol) gave **38a** as a white solid which was further purified by RP-HPLC (3 mg, 66%, $R_f = 0.30$, TLC eluent = 5% methanol in dichloromethane; RP-HPLC (C18) $R_t = 43.8$ min, water/acetonitrile 50/50 \rightarrow 10/90 in 40 min at 5 mL/min). $^1\text{H NMR}$ (400 MHz, CD_3OD) δ 8.34 (s, 1H), 7.62–7.49 (m, 4H), 7.46 (dq, $J = 1.0, 7.0$ Hz, 3H), 7.32–7.21 (m, 3H), 7.07–6.97 (m, 1H), 3.80 (dt, $J = 1.3, 6.3$ Hz, 1H), 2.19 (q, $J = 7.2$ Hz, 1H), 1.92 (t, $J = 5.2$ Hz, 1H), 1.81 (ddd, $J = 1.4, 4.8, 9.1$ Hz, 1H), 1.43 (d, $J = 7.4$ Hz, 2H), 1.21 (ddd, $J = 1.8, 5.4, 9.0$ Hz, 1H). $^{13}\text{C NMR}$ (101 MHz, CD_3OD) δ 155.44, 152.66, 152.18, 140.38, 136.00, 130.36, 130.28, 129.90, 128.75, 126.02, 124.25, 121.26, 116.76, 103.85, 77.89, 77.12, 43.13, 30.78, 30.35, 19.94, 16.73. HRMS m/z $[\text{M} + \text{H}]^+$ for $\text{C}_{25}\text{H}_{24}\text{N}_4\text{O}_2$ calculated 413.1978, found 413.1977.

(1*R*,2*S*,3*R*,4*S*,5*S*)-1-(4-((4-Fluorophenyl)amino)-5-phenyl-7*H*-pyrrolo[2,3-*d*]pyrimidin-7-yl)-4-methylbicyclo[3.1.0]hexane-2,3-diol (**38b**). Following the procedure described for the synthesis of **28**, compound **37b** (5 mg, 0.011 mmol) gave **38b** as a white solid which was purified further by RP-HPLC (2.4 mg, 53%, $R_f = 0.3$, TLC eluent = 5% methanol in dichloromethane; RP-HPLC (C18) $R_t = 42.7$ min, water/acetonitrile 50/50 \rightarrow 10/90 in 40 min at 5 mL/min). $^1\text{H NMR}$ (400 MHz, CD_3OD) δ 8.32 (s, 1H), 7.61–7.50 (m, 4H), 7.50–7.40 (m, 3H), 7.24 (s, 1H), 7.05–6.97 (m, 2H), 4.85–4.82 (m, 1H), 3.80 (dt, $J = 1.3, 6.3$ Hz, 1H), 2.23–2.15 (m, 1H), 1.95–1.89 (m, 1H), 1.81 (ddd, $J = 1.4, 4.7, 9.3$ Hz, 1H), 1.43 (d, $J = 7.4$ Hz, 3H), 1.21 (ddd, $J = 1.9, 5.4, 9.1$ Hz, 1H). $^{19}\text{F NMR}$ (376 MHz, CD_3OD) δ –121.81 (tt, $J = 4.8, 8.4$ Hz). HRMS m/z $[\text{M} + \text{H}]^+$ for $\text{C}_{25}\text{H}_{23}\text{FN}_4\text{O}_2$ calculated 431.1883, found 431.1881.

(1*R*,2*S*,3*R*,4*S*,5*S*)-1-(5-(4-Fluorophenyl)-4-(phenylamino)-7*H*-pyrrolo[2,3-*d*]pyrimidin-7-yl)-4-methylbicyclo[3.1.0]hexane-2,3-diol (**38c**). Following the procedure described for the synthesis of **28**, compound **37c** (7 mg, 0.015 mmol) gave **38c** as a white solid which was purified further by RP-HPLC (4 mg, 63%, $R_f = 0.3$, TLC eluent = 5% methanol in dichloromethane; RP-HPLC (C18) $R_t = 41.9$ min, water/acetonitrile 50/50 \rightarrow 10/90 in 40 min at 5 mL/min). **38c** was soluble in chloroform but not methanol. $^1\text{H NMR}$ (400 MHz, $\text{DMSO-}d_6$) δ 8.37 (s, 1H), 7.63–7.48 (m, 5H), 7.37–7.23 (m, 5H), 6.98 (tt, $J = 1.2, 7.4$ Hz, 1H), 4.78–4.73 (m, 1H), 3.63 (d, $J = 6.1$ Hz, 1H), 2.10–2.02 (m, 1H), 1.72 (t, $J = 5.0$ Hz, 1H), 1.67–1.62 (m, 1H), 1.37 (d, $J = 7.4$ Hz, 3H), 1.24–1.16 (m, 1H). $^{19}\text{F NMR}$ (376 MHz, $\text{DMSO-}d_6$) δ –115.78 (tt, $J = 5.5, 9.1$ Hz). HRMS m/z $[\text{M} + \text{H}]^+$ for $\text{C}_{25}\text{H}_{23}\text{FN}_4\text{O}_2$ calculated 431.1883, found 431.1887.

(3*aS*,3*bR*,4*aS*,5*R*,5*aR*)-3*b*-(4-Amino-5-iodo-7*H*-pyrrolo[2,3-*d*]pyrimidin-7-yl)-2,2-dimethylhexahydrocyclopropa[3,4]cyclopenta[1,2-*d*][1,3]dioxol-5-yl)methanol (**39**). Following the reaction proce-

dure described for the synthesis of **35**, compound **29** (65 mg, 0.095 mmol) gave **39** as a white solid (45 mg, quantitative yield, $R_f = 0.20$, TLC eluent = 5% methanol in dichloromethane). ^1H NMR (400 MHz, CDCl_3) δ 8.23 (s, 1H), 7.19 (s, 1H), 6.81 (dd, $J = 1.8, 12.5$ Hz, 1H), 5.70 (s, 3H), 4.94 (dd, $J = 1.8, 6.9$ Hz, 1H), 4.83 (dd, $J = 1.5, 6.9$ Hz, 1H), 4.05 (dt, $J = 1.5, 11.5$ Hz, 1H), 3.91–3.78 (m, 1H), 2.51–2.42 (m, 1H), 2.01 (ddd, $J = 1.5, 5.2, 9.7$ Hz, 1H), 1.58–1.53 (m, 4H), 1.27 (s, 3H), 1.23 (ddd, $J = 1.9, 5.5, 9.7$ Hz, 1H). HRMS m/z $[\text{M} + \text{H}]^+$ for $\text{C}_{16}\text{H}_{19}\text{IN}_4\text{O}_3$ calculated 443.0580, found 443.0585.

((3*aS*,3*bS*,4*aS*,5*R*,5*aR*)-3*b*-(5-iodo-4-((triphenyl-15-phosphanylidene)amino)-7*H*-pyrrolo[2,3-*d*]pyrimidin-7-yl)-2,2-dimethylhexahydrocyclopropa[3,4]cyclopenta[1,2-*d*][1,3]dioxol-5-yl)methyl Diphenyl Phosphate (**40**). To an ice-cold solution of **39** (20 mg, 0.045 mmol) and triphenylphosphine (17 mg, 0.063 mmol) in anhydrous THF (1 mL) was added diisopropyl azodicarboxylate (DIAD, 13 μL , 0.063 mmol) dropwise. After 5 min, diphenylphosphorylazide (DPPA, 14 μL , 0.063 mmol) was added and stirred at 0 °C for 30 min and then at room temperature overnight. The reaction mixture was heated to 60 °C for 4 h. Solvents were evaporated to dryness, and residue was suspended in ethyl acetate, washed with water and brine, and dried over anhydrous Na_2SO_4 . Solvent was evaporated and the residue purified by silica gel flash column chromatography to afford the product **40** as a white solid ($R_f = 0.80$, TLC eluent = 5% methanol in dichloromethane). ^1H NMR (400 MHz, CD_3OD) δ 7.98–7.88 (m, 4H), 7.86 (s, 1H), 7.63 (s, 1H), 7.55 (ddd, $J = 1.6, 5.2, 7.3$ Hz, 2H), 7.47 (ddd, $J = 3.3, 6.8, 8.7$ Hz, 5H), 7.36–7.08 (m, 12H), 7.07–6.98 (m, 2H), 4.89 (dd, $J = 1.6, 7.2$ Hz, 1H), 4.69–4.63 (m, 2H), 4.54–4.48 (m, 1H), 2.55 (t, $J = 6.9$ Hz, 1H), 1.83–1.75 (m, 1H), 1.57–1.40 (m, 5H), 1.14 (s, 3H). HRMS m/z $[\text{M} + \text{H}]^+$ for $\text{C}_{46}\text{H}_{42}\text{IN}_4\text{O}_6\text{P}_2$ calculated 935.1624, found 935.1628.

N-(7-((3*aS*,3*bS*,4*aS*,5*R*,5*aR*)-5-(Azidomethyl)-2,2-dimethyltetrahydrocyclopropa[3,4]-cyclopenta[1,2-*d*][1,3]dioxol-3*b*(3*aH*)-yl)-5-iodo-7*H*-pyrrolo[2,3-*d*]pyrimidin-4-yl)-1,1,1-triphenyl-15-phosphanimine (**41**). The intermediate compound **40** was dissolved in anhydrous DMF and treated with excess of NaN_3 . The mixture was heated to 65 °C overnight. Solvent was evaporated, and the residue was purified by silica gel flash column chromatography to afford the title compound **41** as a white solid ($R_f = 0.30$, TLC eluent = 20% ethyl acetate in hexanes). ^1H NMR (400 MHz, CDCl_3) δ 8.02–7.91 (m, 7H), 7.55–7.49 (m, 3H), 7.48–7.40 (m, 6H), 7.05 (s, 1H), 5.07 (dd, $J = 1.6, 7.1$ Hz, 1H), 4.54 (dd, $J = 1.4, 7.1$ Hz, 1H), 3.85 (qd, $J = 8.1, 12.1$ Hz, 2H), 2.41 (t, $J = 8.1$ Hz, 1H), 1.86 (ddd, $J = 1.4, 5.4, 9.7$ Hz, 1H), 1.55 (s, 3H), 1.49 (t, $J = 5.6$ Hz, 1H), 1.41 (ddd, $J = 1.7, 5.8, 9.7$ Hz, 1H), 1.22 (s, 3H). HRMS m/z $[\text{M} + \text{H}]^+$ for $\text{C}_{34}\text{H}_{32}\text{IN}_7\text{O}_2\text{P}$ calculated 728.1400, found 728.1406.

7-((3*aS*,3*bS*,4*aS*,5*R*,5*aR*)-5-(Azidomethyl)-2,2-dimethyltetrahydrocyclopropa[3,4]-cyclopenta[1,2-*d*][1,3]dioxol-3*b*(3*aH*)-yl)-5-iodo-7*H*-pyrrolo[2,3-*d*]pyrimidin-4-amine (**42**). To a solution of compound **41** (15 mg, 0.034 mmol) in anhydrous pyridine (0.5 mL) under a nitrogen atmosphere was added methanesulfonyl chloride (MsCl , 6 μL , 0.068 mmol) at 0 °C. After stirring the reaction mixture for 4 h, volatiles were evaporated under vacuum and the residue partitioned between water and ethyl acetate (3 \times 5 mL). The organic layer was separated, combined, dried over anhydrous Na_2SO_4 , and the solvent evaporated. The residue was dissolved in anhydrous DMF (0.5 mL), sodium azide (22 mg, 0.34 mmol) was added, and the mixture was heated to 60 °C for 4 h. The solvent was evaporated under high vacuum, and the residue was suspended in ethyl acetate, washed with water and brine, and dried over anhydrous Na_2SO_4 . The residue after evaporation was purified by silica gel flash column chromatography to afford title compound **42** as a white foamy solid (15 mg, 95%, $R_f = 0.45$, TLC eluent = 5% methanol in dichloromethane). ^1H NMR (400 MHz, CDCl_3) δ 8.24 (s, 1H), 7.12 (s, 1H), 5.63 (s, 2H), 5.08 (dd, $J = 1.7, 7.1$ Hz, 1H), 4.57 (dd, $J = 1.4, 7.1$ Hz, 1H), 3.92 (dd, $J = 7.9, 12.1$ Hz, 1H), 3.83 (dd, $J = 8.3, 12.1$ Hz, 1H), 2.46 (t, $J = 8.1$ Hz, 1H), 1.95 (ddd, $J = 1.4, 5.4, 9.8$ Hz, 1H), 1.59–1.52 (m, 4H), 1.41 (ddd, $J = 1.7, 5.9, 9.8$ Hz, 1H), 1.25 (s, 3H). HRMS m/z $[\text{M} + \text{H}]^+$ for $\text{C}_{16}\text{H}_{18}\text{IN}_7\text{O}_2$ calculated 468.0645, found 468.0647.

(1*S*,2*S*,3*R*,4*R*,5*S*)-1-(4-Amino-5-iodo-7*H*-pyrrolo[2,3-*d*]pyrimidin-7-yl)-4-(azidomethyl)bicyclo[3.1.0]hexane-2,3-diol (**43**). Following

the reaction procedure described for the synthesis of **28**, compound **42** (8 mg, 0.017 mmol) gave **43** as a white solid which was further purified by RP-HPLC (3.1 mg, 42%, $R_f = 0.25$, TLC eluent = 5% methanol in dichloromethane; RP-HPLC (C18) $R_t = 28.5$ min, water/acetonitrile 75/25 \rightarrow 25/75 in 40 min at 5 mL/min). ^1H NMR (400 MHz, CD_3OD) δ 8.11 (s, 1H), 7.31 (s, 1H), 4.66 (dd, $J = 1.9, 6.5$ Hz, 1H), 3.94–3.84 (m, 2H), 3.73 (dd, $J = 7.4, 12.2$ Hz, 1H), 2.30–2.22 (m, 1H), 1.91–1.81 (m, 2H), 1.23–1.17 (m, 1H). HRMS m/z $[\text{M} + \text{H}]^+$ for $\text{C}_{13}\text{H}_{14}\text{IN}_7\text{O}_2$ calculated 428.0332, found 428.0336.

7-((3*aS*,3*bS*,4*aS*,5*R*,5*aR*)-5-(Aminomethyl)-2,2-dimethyltetrahydrocyclopropa[3,4]-cyclopenta[1,2-*d*][1,3]dioxol-3*b*(3*aH*)-yl)-5-iodo-7*H*-pyrrolo[2,3-*d*]pyrimidin-4-amine (**44**). Compound **42** (8 mg, 0.017 mmol) was dissolved in anhydrous THF (0.5 mL) and to this was added triphenylphosphine (9 mg, 0.034 mmol) and then stirred at room temperature overnight. Ammonium hydroxide (25%, 30 μL) was added and heated to 65 °C under reflux condenser for 4 h. Solvent was evaporated, and the residue was purified by silica gel flash column chromatography to afford **44** (6 mg, 80%, $R_f = 0.10$, TLC eluent = 10% methanol and 1% triethylamine in dichloromethane). HRMS m/z $[\text{M} + \text{H}]^+$ for $\text{C}_{16}\text{H}_{20}\text{IN}_5\text{O}_2$ calculated 442.0740, found 442.0736.

(1*S*,2*S*,3*R*,4*R*,5*S*)-1-(4-Amino-5-iodo-7*H*-pyrrolo[2,3-*d*]pyrimidin-7-yl)-4-(aminomethyl)bicyclo[3.1.0]hexane-2,3-diol acetate (**45**). Following the reaction procedure described for the synthesis of **28**, compound **44** (6 mg, 0.0136 mmol) after purification by RP-HPLC gave **45** as a white solid (1.91 mg, 35%. RP-HPLC (C18) $R_t = 29.6$ min, 10 mM triethylammonium acetate in water/acetonitrile 90/10 \rightarrow 65/35 in 40 min at 5 mL/min). ^1H NMR (400 MHz, CD_3OD) δ 8.11 (s, 1H), 7.34 (s, 1H), 4.56 (d, $J = 6.8$ Hz, 1H), 4.00 (d, $J = 6.6$ Hz, 1H), 3.38 (t, $J = 5.9$ Hz, 2H), 2.43 (t, $J = 5.0$ Hz, 1H), 1.95–1.70 (m, 5H), 1.27 (t, $J = 7.2$ Hz, 1H). HRMS m/z $[\text{M} + \text{H}]^+$ for $\text{C}_{13}\text{H}_{16}\text{IN}_5\text{O}_2$ calculated 402.0427, found 402.0421.

(3*aS*,3*bS*,4*aS*,5*S*,5*aR*)-3*b*-(4-Amino-5-iodo-7*H*-pyrrolo[2,3-*d*]pyrimidin-7-yl)-2,2-dimethylhexahydrocyclopropa[3,4]cyclopenta[1,2-*d*][1,3]dioxole-5-carboxylic Acid (**46**). To a solution of compound **39** (40 mg, 0.09 mmol) in acetonitrile–water (4:1, 2.0 mL) was added bis(acetoxy)iodobenzene (BAIB, 64 mg, 0.20 mmol) and 2,2,6,6-tetramethylpiperidine-1-oxyl (TEMPO, 12 mg, 0.077 mmol) at room temperature. After stirring for 18 h at room temperature, the volatiles were evaporated under high vacuum. The residue was purified by silica gel column chromatography to afford **46** as a light-yellow solid (20 mg, 49%, $R_f = 0.20$, TLC eluent = 5% methanol in dichloromethane). ^1H NMR (400 MHz, CDCl_3) δ 8.23 (s, 1H), 7.21 (s, 1H), 6.10 (s, 2H), 5.02 (dd, $J = 1.7, 7.1$ Hz, 1H), 4.94 (dt, $J = 1.2, 6.8$ Hz, 1H), 3.30 (s, 1H), 2.31 (ddd, $J = 1.5, 5.3, 10.0$ Hz, 1H), 1.67 (t, $J = 5.7$ Hz, 1H), 1.57 (s, 3H), 1.48 (ddd, $J = 1.8, 6.0, 9.9$ Hz, 1H), 1.25 (s, 4H). HRMS m/z $[\text{M} + \text{H}]^+$ for $\text{C}_{16}\text{H}_{17}\text{IN}_4\text{O}_4$ calculated 457.0373, found 457.0381.

1,3-Bis((1*S*,2*S*,3*R*,4*S*,5*S*)-5-(4-Amino-5-iodo-7*H*-pyrrolo[2,3-*d*]pyrimidin-7-yl)-3,4-dihydroxybicyclo[3.1.0]hexan-2-yl)urea (**47**). ^1H NMR (400 MHz, CD_3OD) δ 8.21 (s, 1H), 7.35 (s, 1H), 4.74 (dd, $J = 2.1, 6.3$ Hz, 1H), 4.19 (s, 1H), 3.92–3.86 (m, 1H), 2.91–2.77 (m, 6H), 2.04 (t, $J = 5.4$ Hz, 1H), 1.88 (s, 4H), 1.28 (td, $J = 3.6, 6.3, 7.2$ Hz, 2H), 1.16 (t, $J = 7.3$ Hz, 9H). HRMS m/z $[\text{M} + \text{H}]^+$ for $\text{C}_{25}\text{H}_{26}\text{I}_2\text{N}_{10}\text{O}_5$ calculated 801.0255, found 801.0250.

Benzyl ((3*aS*,3*bS*,4*aS*,5*S*,5*aR*)-3*b*-(4-Amino-5-iodo-7*H*-pyrrolo[2,3-*d*]pyrimidin-7-yl)-2,2-dimethylhexahydrocyclopropa[3,4]cyclopenta[1,2-*d*][1,3]dioxol-5-yl)carbamate (**48**). To a solution of compound **46** (20 mg, 0.0437 mmol) in anhydrous THF (0.5 mL) was added triethylamine (12 μL , 0.0875 mmol) and diphenylphosphoryl azide (DPPA, 15 μL , 0.065 mmol) at room temperature. After stirring overnight at room temperature, the solvent was evaporated under reduced pressure and the residue was dissolved in anhydrous toluene (1.0 mL). To this mixture was added benzyl alcohol (50 μL , 0.48 mmol) and heated to 120 °C for 5 h. The volatile compounds were evaporated under reduced pressure and the residue purified by silica gel column chromatography to afford **48** as a light-yellow solid (4.0 mg, 17%, $R_f = 0.65$, TLC eluent = 5% methanol in dichloromethane). ^1H NMR (400 MHz, CDCl_3) δ 8.22 (s, 1H), 7.56 (d, $J = 8.8$ Hz, 2H), 7.49–7.29 (m, 4H), 7.15 (s, 1H), 5.78 (s, 2H), 5.25–5.12 (m, 2H), 4.96 (dd, $J = 1.9, 6.7$ Hz, 1H), 4.59 (dd, $J =$

1.9, 6.6 Hz, 1H), 4.36 (d, $J = 8.7$ Hz, 1H), 1.97 (ddd, $J = 1.9, 5.8, 10.3$ Hz, 1H), 1.66 (t, $J = 6.0$ Hz, 1H), 1.55 (s, 3H), 1.41 (ddd, $J = 1.9, 6.3, 10.3$ Hz, 1H), 1.22 (s, 3H). HRMS m/z $[M + H]^+$ for $C_{23}H_{24}IN_3O_4$ calculated 562.0951, found 562.0955.

(1*S*,2*S*,3*R*,4*S*,5*S*)-4-Amino-1-(4-amino-5-iodo-7*H*-pyrrolo[2,3-*d*]pyrimidin-7-yl)bicyclo[3.1.0]hexane-2,3-diol (**49**). To a solution of compound **48** (3.0 mg, 5.34 μ mol) in anhydrous dichloromethane (0.1 mL) was added 33% HBr in acetic acid (5 μ L, 27.5 μ mol) at 0 °C and stirred at room temperature for 0.5 h. The volatiles were evaporated under vacuum, and the residual acid was chased by evaporating repeatedly with dichloromethane (HRMS indicated 2',3'-isopropylidene deprotected compound). The above procedure was repeated and stirred for 1.5 h [Note: a straight 2 h reaction degraded the starting material]. The volatiles were evaporated under vacuum, and the residual acid was removed by evaporating repeatedly with dichloromethane. The product mixture was dissolved in methanol and subjected to RP-HPLC (C18) purification to afford **49** and **50** as a white solid. Compound **49** acetate salt (0.35 mg, 17%; RP-HPLC (C18) $R_t = 29.4$ min, 10 mM triethylammonium acetate in water/acetonitrile 90/10 \rightarrow 65/35 in 40 min at 5 mL/min). 1H NMR (400 MHz, CD_3OD) δ 8.13 (s, 1H), 7.33 (s, 1H), 4.81 (dd, $J = 2.2, 6.4$ Hz, 1H), 3.90 (dd, $J = 1.9, 6.4$ Hz, 1H), 1.95 (t, $J = 5.5$ Hz, 1H), 1.88–1.81 (m, 1H), 1.35–1.25 (m, 2H). HRMS m/z $[M + H]^+$ for $C_{12}H_{14}IN_3O_2$ calculated 388.0270, found 388.0268. (1*R*,2*S*,3*R*,4*S*,5*S*)-4-amino-1-(4-amino-7*H*-pyrrolo[2,3-*d*]pyrimidin-7-yl)bicyclo[3.1.0]hexane-2,3-diol (**50**): RP-HPLC (C18) $R_t = 15.8$ min, 10 mM triethylammonium acetate in water/acetonitrile 90/10 \rightarrow 65/35 in 40 min at 5 mL/min). 1H NMR (400 MHz, CD_3OD) δ 8.10 (s, 1H), 7.13 (d, $J = 3.6$ Hz, 1H), 6.51 (d, $J = 3.6$ Hz, 1H), 4.86–4.83 (m, 1H), 3.96–3.88 (m, 1H), 1.95 (dd, $J = 5.0, 5.8$ Hz, 1H), 1.83 (ddd, $J = 1.9, 5.0, 9.5$ Hz, 1H), 1.30 (ddd, $J = 2.0, 5.7, 9.3$ Hz, 1H). HRMS m/z $[M + H]^+$ for $C_{12}H_{15}N_3O_2$ calculated 262.1299, found 262.1303.

7-((3*aR*,3*bR*,4*aS*,5*R*,5*aS*)-3*b*-(((*tert*-Butyldiphenylsilyl)oxy)methyl)-2,2-dimethylhexahydrocyclopropa[3,4]cyclopenta[1,2-*d*]-[1,3]dioxol-5-yl)-4-chloro-5-iodo-7*H*-pyrrolo[2,3-*d*]pyrimidine (**52**). Compound **51** (46 mg, 0.105 mmol) was dried by evaporating with anhydrous toluene (2 \times 1 mL). To the dried compound was added anhydrous THF (1 mL), triphenylphosphine (83 mg, 0.315 mmol), and 6-chloro-7-iodo-7-deazapurine (88 mg, 0.315 mmol). The mixture was cooled to 0 °C and diisopropylazodicarboxylate (62 μ L, 0.315 mmol) added dropwise. After 30 min, the reaction mixture was brought to room temperature and stirred overnight (18 h). The volatiles were evaporated under reduced pressure and the residue purified by silica gel chromatography to afford **52** as light-yellow foam (65 mg, 88%, $R_f = 0.55$, TLC eluent = 20% ethyl acetate in hexanes). 1H NMR (400 MHz, $CDCl_3$) δ 8.61 (s, 1H), 7.74 (s, 1H), 7.71–7.63 (m, 4H), 7.47–7.34 (m, 6H), 5.35 (s, 1H), 5.31 (dd, $J = 1.4, 7.3$ Hz, 1H), 4.51–4.45 (m, 1H), 4.29 (dd, $J = 0.7, 11.0$ Hz, 1H), 3.42 (d, $J = 11.0$ Hz, 1H), 1.60 (ddd, $J = 1.5, 4.4, 9.3$ Hz, 1H), 1.53 (s, 3H), 1.23 (s, 3H), 1.12–1.15 (m, 1H), 1.16 (s, 9H), 0.92–0.84 (m, 1H). HRMS m/z $[M + H]^+$ for $C_{32}H_{35}ClIN_4O_3Si$ calculated 700.1259, found 700.1266.

7-((3*aR*,3*bR*,4*aS*,5*R*,5*aS*)-3*b*-(((*tert*-Butyldiphenylsilyl)oxy)methyl)-2,2-dimethylhexahydrocyclopropa[3,4]cyclopenta[1,2-*d*]-[1,3]dioxol-5-yl)-5-iodo-*N*-phenyl-7*H*-pyrrolo[2,3-*d*]pyrimidin-4-amine (**53**). Following the procedure described for the synthesis of **31a**, compound **52** (125 mg, 0.178 mmol) gave **53** as a white foam (85 mg, 63%, $R_f = 0.3$, TLC eluent = 10% ethyl acetate in hexanes). 1H NMR (400 MHz, $CDCl_3$) δ 8.47 (s, 1H), 8.19 (s, 1H), 7.79–7.64 (m, 6H), 7.53 (s, 1H), 7.48–7.34 (m, 8H), 7.20–7.13 (m, 1H), 5.36 (s, 1H), 5.33 (dd, $J = 1.4, 7.2$ Hz, 1H), 4.49 (dd, $J = 1.5, 7.2$ Hz, 1H), 4.32 (d, $J = 11.2$ Hz, 1H), 3.36 (d, $J = 11.1$ Hz, 1H), 1.62 (ddd, $J = 1.5, 4.4, 9.3$ Hz, 1H), 1.52 (s, 3H), 1.24 (s, 3H), 1.17 (s, 8H), 1.16–1.13 (m, 1H), 0.83 (ddd, $J = 1.5, 5.6, 9.3$ Hz, 1H). HRMS m/z $[M + H]^+$ for $C_{38}H_{41}IN_4O_3Si$ calculated 757.2071, found 757.2072.

7-((3*aR*,3*bR*,4*aS*,5*R*,5*aS*)-3*b*-(((*tert*-Butyldiphenylsilyl)oxy)methyl)-2,2-dimethylhexahydrocyclopropa[3,4]cyclopenta[1,2-*d*]-[1,3]dioxol-5-yl)-*N*,5-diphenyl-7*H*-pyrrolo[2,3-*d*]pyrimidin-4-amine (**54**). Following the procedure described for the synthesis of **33a**, compound **53** (85 mg, 0.112 mmol) gave **54** as a white foam (65 mg, 82%, $R_f = 0.25$, TLC eluent = 10% ethyl acetate in hexanes). 1H NMR

(400 MHz, $CDCl_3$) δ 8.53 (s, 1H), 7.66–7.56 (m, 4H), 7.50 (d, $J = 8.0$ Hz, 3H), 7.45–7.34 (m, 7H), 7.34–7.24 (m, 6H), 7.07–7.00 (m, 1H), 5.45 (s, 1H), 5.36 (dd, $J = 1.4, 7.2$ Hz, 1H), 4.62 (dd, $J = 1.5, 7.3$ Hz, 1H), 4.29 (d, $J = 11.0$ Hz, 1H), 3.41 (d, $J = 11.0$ Hz, 1H), 1.76 (ddd, $J = 1.5, 4.4, 9.3$ Hz, 1H), 1.55 (s, 3H), 1.27 (s, 3H), 1.18 (dd, $J = 4.4, 5.6$ Hz, 1H), 0.94 (s, 9H), 0.92–0.83 (m, 1H). HRMS m/z $[M + H]^+$ for $C_{44}H_{46}N_4O_3Si$ calculated 707.3417, found 707.3414.

(1*R*,2*R*,3*S*,4*R*,5*S*)-1-(Hydroxymethyl)-4-(5-phenyl-4-(phenylamino)-7*H*-pyrrolo[2,3-*d*]pyrimidin-7-yl)bicyclo[3.1.0]hexane-2,3-diol (**55**). Following the procedure described for the synthesis of **28**, compound **54** (15 mg, 0.021 mmol) afforded **55** as a white solid which was further purified by RP-HPLC (7 mg, 77%, $R_f = 0.15$, TLC eluent = 5% methanol in dichloromethane; RP-HPLC (C18) $R_t = 24.9$ min, water/acetonitrile 50/50 \rightarrow 10/90 in 40 min at 5 mL/min). 1H NMR (400 MHz, 9:1 CD_3OD - $CDCl_3$) δ 8.34 (s, 1H), 7.75 (d, $J = 1.8$ Hz, 1H), 7.63–7.40 (m, 7H), 7.28 (t, $J = 7.7$ Hz, 2H), 7.03 (td, $J = 1.1, 7.4$ Hz, 1H), 5.11 (s, 1H), 4.80 (dd, $J = 1.5, 6.8$ Hz, 1H), 4.28 (d, $J = 11.7$ Hz, 1H), 3.87 (dd, $J = 1.3, 6.8$ Hz, 1H), 3.28 (d, $J = 6.9$ Hz, 1H), 1.63 (dd, $J = 3.8, 8.9$ Hz, 1H), 1.54 (t, $J = 4.6$ Hz, 1H), 0.77–0.69 (m, 1H). ^{13}C NMR (101 MHz, 9:1 CD_3OD - $CDCl_3$) δ 155.20, 151.61, 150.10, 139.46, 135.42, 129.94, 129.93, 129.63, 128.42, 124.27, 122.91, 121.24, 116.99, 103.22, 77.84, 72.04, 64.34, 63.18, 37.74, 24.46, 11.96. HRMS m/z $[M + H]^+$ for $C_{25}H_{24}N_4O_3$ calculated 429.1927, found 429.1924.

7-((3*aR*,3*bR*,4*aS*,5*R*,5*aS*)-3*b*-(((*tert*-Butyldiphenylsilyl)oxy)methyl)-2,2-dimethylhexahydrocyclopropa[3,4]cyclopenta[1,2-*d*]-[1,3]dioxol-5-yl)-5-iodo-7*H*-pyrrolo[2,3-*d*]pyrimidin-4-amine (**56**). Following the procedure described for the synthesis of **29**, compound **52** (20 mg, 0.028 mmol) gave **56** as a white foam (16 mg, 82%, $R_f = 0.45$, TLC eluent = 50% ethyl acetate in hexanes). 1H NMR (400 MHz, $CDCl_3$) δ 8.25 (s, 1H), 7.76–7.60 (m, 4H), 7.49 (s, 1H), 7.47–7.33 (m, 6H), 6.20 (s, 2H), 5.37–5.26 (m, 2H), 4.53–4.40 (m, 1H), 4.30 (d, $J = 11.0$ Hz, 1H), 3.36 (d, $J = 11.0$ Hz, 1H), 1.59 (ddd, $J = 1.5, 4.4, 9.3$ Hz, 1H), 1.51 (s, 3H), 1.25–1.21 (m, 3H), 1.16 (s, 9H), 1.13 (dd, $J = 4.5, 5.7$ Hz, 1H), 0.82 (ddd, $J = 1.5, 5.6, 9.3$ Hz, 1H). HRMS m/z $[M + H]^+$ for $C_{32}H_{37}IN_4O_3Si$ calculated 681.1758, found 681.1769.

(1*R*,2*R*,3*S*,4*R*,5*S*)-4-(4-Amino-5-iodo-7*H*-pyrrolo[2,3-*d*]pyrimidin-7-yl)-1-(hydroxymethyl)bicyclo[3.1.0]hexane-2,3-diol (**57**). Following the procedure described for the synthesis of **28**, compound **56** (16 mg, 0.019 mmol) afforded **57** as a white solid (7.5 mg, 79%, $R_f = 0.25$, TLC eluent = 10% methanol in dichloromethane). 1H NMR (400 MHz, CD_3OD) δ 8.11 (s, 1H), 7.79 (s, 1H), 4.99 (s, 1H), 4.72 (dd, $J = 1.6, 6.7$ Hz, 1H), 4.26 (dd, $J = 1.0, 11.7$ Hz, 1H), 3.74 (dt, $J = 1.2, 6.7$ Hz, 1H), 3.33 (d, $J = 15.5$ Hz, 1H), 3.27 (d, $J = 11.7$ Hz, 1H), 1.57–1.43 (m, 2H), 0.70 (ddd, $J = 1.8, 4.5, 8.0$ Hz, 1H). ^{13}C NMR (101 MHz, CD_3OD) δ 158.81, 152.52, 150.32, 129.15, 105.15, 78.26, 72.29, 64.43, 63.50, 50.37, 37.97, 24.66, 12.12. HRMS m/z $[M + H]^+$ for $C_{13}H_{15}IN_4O_3$ calculated 403.0267, found 403.0271.

Quantification of hAdK Inhibition. The nucleoside derivatives were tested for inhibitory activity at hAdK using a commercial kit for the measurement of hAdK activity (ADK Phosphorylation Assay Kit, ref. no. K0507-02, NovoCib, Lyon, France). For use in the assay, compounds **28**, **30**, **32**, **43**, **45**, and **49** were dissolved in 60% DMSO in purified water, **34** was prepared in 80% DMSO solution, and **38a** was prepared in 88% DMSO solution, while **38b**, **38c**, **55**, and **57** were prepared in 100% DMSO. Reactions were performed at 37 °C in a total volume of 200 μ L containing 100 mM Tris/HCl, 250 mM KCl, 10 mM $MgCl_2$, 2.5 mM NAD, 2.75 mM ATP, 20 mU/mL IMPDH, 2.2 mU hAdK. All assays were run in triplicate and then replicated on a different plate. hAdK activity was assayed by measuring specific absorption at 340 nm at 5 min time intervals using a Spectromax plate reader (Molecular Devices, CA, USA). All reactions were started by the addition of 2.5 mM inosine (t_0) and maintained for a total of 4 h. Baseline absorption prior to the addition of inosine was subtracted from all measurements. Percent inhibition of hAdK activity was calculated based on the slope during the linear phase of the progression of the enzymatic reaction (quantified between 0 and 40 min after inosine addition) and normalized to the slope of the enzymatic reaction in the presence of the vehicle DMSO (1% v/v final concentration of reaction mix).

Statistical Analysis. Two-way ANOVA was used to determine significances between compound and concentration with percent residual hAdK activity based on slope as the primary dependent measure. Slopes were calculated for the first 40 min of activity for each compound and concentration combination. Post hoc analyses were used to determine specific between group differences relative to 2 using Bonferroni multiple corrections test.

Molecular Modeling. Computational Facilities. Ligand geometry optimization and molecular docking simulations were carried out using a 8 Intel Xeon X5482 CPU workstation. Membrane MD simulations were run on four NVIDIA Tesla K20X by exploiting the computational resources of the NIH HPC Biowulf cluster (<http://biowulf.nih.gov>).

Ligand Preparation. The compounds were built using Maestro⁵⁶ and subjected to gas phase geometry optimization with the Jaguar 8.9 quantum chemistry package⁵⁷ using density functional theory (DFT) with the B3LYP hybrid functional and the 6-31G** (34 and 55) or LACVP** (1c, 1a, 30, and 57) basis set. Frequency calculations were performed to ensure the structures represented minima on the potential energy surfaces.

Protein Preparation. The structure of hAdK in complex with 1c was retrieved from the RCSB PDB database⁵⁸ (<http://www.rcsb.org>, PDB ID 2I6A) and prepared as follows: after manual removal of cocrystallized ligand and water molecules, ionization states of protein side chains and hydrogen positions were assigned with the Protein Preparation Wizard tool.⁵⁹

Induced Fit Docking. The ligands were docked by means of the IFD procedure based on Glide search algorithm⁶⁰ using the Standard Protocol and OPLS3 force field.⁶¹ The centroid of the cocrystallized S15 ligand residue was selected as center of the Glide grid (inner box side = 10 Å; outer box side = auto). Ligands were initially docked rigidly into the receptor by applying a scaling factor of 0.5 to both ligand and protein van der Waals radii. Up to 20 poses per ligand were collected and the side chains of residues within 5 Å of the ligand were refined with Prime.⁶² Ligands were redocked into the newly generated receptor conformations with Glide⁶⁰ by generating up to 10 poses using the SP scoring function and reverting the vdW radii scaling factors to their default values.

Molecular Dynamics. MD simulations were carried out with the ACEMD program⁶³ using periodic boundaries conditions and the AMBER14SB⁶⁴/General Amber Force Field (GAFF)⁶⁵ force fields for the protein and ligand atoms, respectively. To derive force field parameters, ligands were subjected to energy minimization with Gaussian 09⁶⁶ at the HF/6-31G* level of theory. After geometry optimization, ligand parameters and RESP partial charges were derived with antechamber and parmchk tools as implemented in amber-tools2014.⁶⁴ Protein–ligand complexes were solvated by a cubic water box with cell borders placed at least 12 Å away from any protein atom using TIP3P as water model.⁶⁷ The systems were neutralized with Na⁺/Cl⁻ counterions to a final salt concentration of 0.150 M. After 2000 steps of energy minimization (conjugate-gradient method), the systems were equilibrated with 50000 steps (100 ps) of NVE followed by 1 ns of NPT simulations by applying harmonic positional constraints on protein and ligand atoms that were gradually reduced (scaling factor = 0.1). During the equilibration, the temperature was maintained at 310 K using a Langevin thermostat⁶⁸ with a low damping constant of 1 ps⁻¹, and the pressure was maintained at 1 atm using a Berendsen barostat.⁶⁹ Bond lengths involving hydrogen atoms were constrained using the M-SHAKE⁷⁰ algorithm with an integration time step of 2 fs. The equilibrated systems were then subjected to 30 ns of unrestrained MD simulations in a NVT ensemble. Long-range Coulomb interactions were handled using the particle mesh Ewald summation method (PME)⁷¹ with mesh spacing set to 1.0 Å. A nonbonded cutoff distance of 9 Å with a switching distance of 7.5 Å was used. Each simulation was run in triplicate.

Trajectory Analysis. Selection of representative trajectories was based upon the total ligand–protein interaction energy (IE_{tot}). In particular, for each ligand–protein system, the IE_{tot} expressed as the sum of van der Waals (IE_{vdw}) and electrostatic (IE_{ele}) contribution was computed at frames extracted every 50 ps with the *mdenergy* function

implemented in VMD⁷² exploiting NAMD 2.10.⁷³ From the IE_{tot} values so obtained, we derived a modified version of the dynamic scoring function⁷⁴ (herein defined as wDSF_{tot}) by computing the cumulative sum of ligand–protein IE_{tot} and dividing the value for the ligand RMSD with respect to the starting conformation as follows:

$$wDSF_{tot} = \sum_{i=1}^n \frac{IE_{tot}}{RMSD}$$

wDSF_{tot} slope values were derived as previously reported,⁷⁴ and for each ligand–protein system the replica that returned the highest absolute slope value (Supporting Information, Table S1) was selected. IE vs simulation time graphs were generated with Gnuplot.⁷⁵

Sugar pseudorotation phase angle⁷⁶ (*P*) during MD simulations was computed with a in house tcl script with the endocyclic torsions ν_0 – ν_4 angles defined as reported in Supporting Information, Figure S6, by using the following equation:

$$P = \tan^{-1} \frac{(\nu_4 + \nu_1) - (\nu_3 + \nu_0)}{2\nu_2(\sin 36^\circ + \sin 72^\circ)}$$

Ligand root-mean-square deviation and fluctuation (RMSD and RMSF, respectively) and protein α carbon atoms RMSD with respect to the starting docking pose were computed with the RMSD trajectory tool (RSMDDT) implemented in VMD. MD average protein structures were derived with the *g_covar* function implemented in GROMACS,^{77,78} and rigid body rotation angles were computed through the DYNDOM web server.⁷⁹

■ ASSOCIATED CONTENT

📄 Supporting Information

The Supporting Information is available free of charge on the ACS Publications website at DOI: 10.1021/acs.jmedchem.6b00689.

Procedures for synthesis of intermediate 24, ¹H NMR and mass spectra of final compounds, supplementary modeling figures (conformational analysis and IE profile of 60 ns of MD simulation of hAdK in complex with 1c, IE profiles of 30 ns of MD simulation of hAdK in complex with 34 and 55, superimposition between average MD and X-ray protein structures, docking pose of 1a and superimposition between average MD and X-ray protein structures, definition of endocyclic torsion angles) and table (MD replicas RMSD and wDSF_{tot} values), and enzymatic assay data (PDF)

3D coordinates of the hAdK in complex with 30 (PDB)

3D coordinates of the hAdK in complex with 57 (PDB)

3D coordinates of the hAdK in complex with 34 (PDB)

3D coordinates of the hAdK in complex with 55 (PDB)

Video S1 of 30 ns of MD simulation of the hAdK in complex with 1c (AVI)

Video S2 of the comparison of 30 ns of MD simulation of the hAdK in complex with 30 and 57 (AVI)

Video S3 of the comparison of 30 ns of MD simulation of the hAdK in complex with 34 and 55 (AVI)

Video S4 of 30 ns of MD simulation of the hAdK in complex with 1a (AVI)

Molecular formula strings (CSV)

■ AUTHOR INFORMATION

Corresponding Author

*Phone: 301-496-9024. Fax: 301-480-8422. E-mail: kajacobsathelix.nih.gov.

Notes

The authors declare no competing financial interest.

ACKNOWLEDGMENTS

We thank Dr. John Lloyd and Dr. Noel Whittaker (NIDDK) for mass spectral determinations. This research was supported by the Intramural Research Program of the NIH, National Institute of Diabetes and Digestive and Kidney Diseases (ZIA DK031117-28), National Institute of Neurological Disorders and Stroke (R21 NS088024), and National Institute of Mental Health (R01 MH083973). We thank Prof. Artem Melman (Clarkson College) for helpful discussions. We thank Dr. Bryan L. Roth (University of North Carolina at Chapel Hill) and National Institute of Mental Health's Psychoactive Drug Screening Program (contract no. HHSN-271-2008-00025-C) for screening data.

ABBREVIATIONS USED

5-IT, 5-iodotubercidin; ADA, adenosine deaminase; AdK, adenosine kinase; AIBN, 2,2'-azobis(2-methylpropionitrile); AMP, adenosine 5'-monophosphate; ATP, adenosine 5'-triphosphate; BAIB, (diacetoxyiodo)benzene; CHO, Chinese hamster ovary; DCM, dichloromethane; DEAD, diethyl azodicarboxylate; DIAD, diisopropyl azodicarboxylate; DIPEA, diisopropylethylamine; DMAP, *N,N*-dimethylaminepyridine; DME, 1,2-dimethoxyethane; DMF, *N,N*-dimethylformamide; DPPA, diphenylphosphoryl azide; ENT1, equilibrative nucleoside transporter1; hAdK, human adenosine kinase; HEPES, 4-(2-hydroxyethyl)-1-piperazineethanesulfonic acid; HRMS, high resolution mass spectroscopy; IE, interaction energy; IFD, induced fit docking; LC-MS, liquid chromatography mass spectroscopy; NAD, nicotinamide adenine dinucleotide; NIS, *N*-iodosuccinimide; NMR, nuclear magnetic resonance; RP-HPLC, reversed phase high pressure liquid chromatography; TBAF, tetrabutylammonium fluoride; TEA, triethylamine; TEMPO, (2,2,6,6-tetramethylpiperidin-1-yl)oxyl; TFA, trifluoroacetic acid; TLC, thin layer chromatography; tPSA, total polar surface area

REFERENCES

- (1) Chen, J. F.; Eltzschig, H. K.; Fredholm, B. B. Adenosine receptors as drug targets - what are the challenges? *Nat. Rev. Drug Discovery* **2013**, *12*, 265–286.
- (2) Wiesner, J. B.; Ugarkar, B. G.; Castellino, A. J.; Barankiewicz, J.; Dumas, D. P.; Gruber, H. E.; Foster, A. C.; Erion, M. D. Adenosine kinase inhibitors as a novel approach to anticonvulsant therapy. *J. Pharmacol. Exp. Ther.* **1999**, *289*, 1669–1677.
- (3) Zylka, M. J. Pain-relieving prospects for adenosine receptors and ectonucleotidases. *Trends Mol. Med.* **2011**, *17*, 188–196.
- (4) Choi, I. Y.; Lee, J. C.; Ju, C.; Hwang, S.; Cho, G. S.; Lee, H. W.; Choi, W. J.; Jeong, L. S.; Kim, W. K. A₃ adenosine receptor agonist reduces brain ischemic injury and inhibits inflammatory cell migration in rats. *Am. J. Pathol.* **2011**, *179*, 2042–2052.
- (5) Williams-Karnesky, R. L.; Sandau, U. S.; Lusardi, T. A.; Lytle, N. K.; Farrell, J. M.; Pritchard, E. M.; Kaplan, D. L.; Boison, D. Epigenetic changes induced by adenosine augmentation therapy prevent epileptogenesis. *J. Clin. Invest.* **2013**, *123*, 3552–3563.
- (6) Zimmermann, H.; Zebisch, M.; Sträter, N. Cellular function and molecular structure of ectonucleotidases. *Purinergic Signalling* **2012**, *8*, 437–502.
- (7) Parkinson, F. E.; Damaraju, V. L.; Graham, K.; Yao, S. Y. M.; Baldwin, S. A.; Cass, C. E.; Young, J. D. Molecular biology of nucleoside transporters and their distributions and functions in the brain. *Curr. Top. Med. Chem.* **2011**, *11*, 948–972.
- (8) Boison, D. Adenosine kinase: exploitation for therapeutic gain. *Pharmacol. Rev.* **2013**, *65*, 906–943.
- (9) Cui, X. A.; Agarwal, T.; Singh, B.; Gupta, R. S. Molecular characterization of Chinese hamster cells mutants affected in

adenosine kinase and showing novel genetic and biochemical characteristics. *BMC Biochem.* **2011**, *12*, 22.

- (10) Fedele, D. E.; Li, T.; Lan, J. Q.; Fredholm, B. B.; Boison, D. Adenosine A₁ receptors are crucial in keeping an epileptic focus localized. *Exp. Neurol.* **2006**, *200*, 184–190.

- (11) Miller-Delaney, S. F.; Bryan, K.; Das, S.; McKiernan, R. C.; Bray, I. M.; Reynolds, J. P.; Gwinn, R.; Stallings, R. L.; Henshall, D. C. Differential DNA methylation profiles of coding and non-coding genes define hippocampal sclerosis in human temporal lobe epilepsy. *Brain* **2015**, *138*, 616–631.

- (12) Boison, D.; Scheurer, L.; Zumsteg, V.; Rülicke, T.; Litynski, P.; Fowler, B.; Brandner, S.; Mohler, H. Neonatal hepatic steatosis by disruption of the adenosine kinase gene. *Proc. Natl. Acad. Sci. U. S. A.* **2002**, *99*, 6985–6990.

- (13) Tosh, D. K.; Paoletta, S.; Deflorian, F.; Phan, K.; Moss, S. M.; Gao, Z. G.; Jiang, X.; Jacobson, K. A. Structural sweet spot for A₁ adenosine receptor activation by truncated (N)-methanocarba nucleosides: Receptor docking and potent anticonvulsant activity. *J. Med. Chem.* **2012**, *55*, 8075–8090.

- (14) Boison, D. Adenosine augmentation therapy for epilepsy. In *Jasper's Basic Mechanisms of the Epilepsies*; Noebels, J. L., Avoli, M., Rogawski, M. A., Olsen, R. W., Delgado-Escueta, A. V., Eds.; Oxford University Press: Oxford, UK, 2012; pp 1150–1160.

- (15) Boison, D.; Huber, A.; Padrun, V.; Deglon, N.; Aebischer, P.; Mohler, H. Seizure suppression by adenosine-releasing cells is independent of seizure frequency. *Epilepsia* **2002**, *43*, 788–796.

- (16) Boison, D.; Singer, P.; Shen, H. Y.; Feldon, J.; Yee, B. K. Adenosine hypothesis of schizophrenia - opportunities for pharmacotherapy. *Neuropharmacology* **2012**, *62*, 1527–1543.

- (17) Ugarkar, B. G.; Castellino, A. J.; Dare, J. M.; Kopcho, J. J.; Wiesner, J. B.; Schanzer, J. M.; Erion, M. D. Adenosine kinase inhibitors. 2. Synthesis, enzyme inhibition, and antiseizure activity of diaryltubercidin analogues. *J. Med. Chem.* **2000**, *43*, 2894–2905.

- (18) Lee, C.-H.; Jiang, M.; Cowart, M.; Gfesser, G.; Perner, R.; Kim, K. H.; Gu, Y. G.; Williams, M.; Jarvis, M. F.; Kowaluk, E. A.; Stewart, A. O.; Bhagwat, S. S. Discovery of 4-amino-5-(3-bromophenyl)-7-(6-morpholino-pyridin-3-yl)pyrido[2,3-d]pyrimidine, an orally active, non-nucleoside adenosine kinase inhibitor. *J. Med. Chem.* **2001**, *44*, 2133–2138.

- (19) (a) McGaraughty, S.; Cowart, M.; Jarvis, M. F. Recent developments in the discovery of novel adenosine kinase inhibitors: Mechanism of action and therapeutic potential. *CNS Drug Rev.* **2001**, *7*, 415–432. (b) Butini, S.; Gemma, S.; Brindisi, M.; Borrelli, G.; Lossani, A.; Ponte, A. M.; Torti, A.; Maga, G.; Marinelli, L.; La Pietra, V.; Fiorini, I.; Lamponi, S.; Campiani, G.; Zisterer, D. M.; Nathani, S. M.; Sartini, S.; La Motta, C.; Da Settimo, F.; Novellino, E.; Foche, F. Non-nucleoside inhibitors of human adenosine kinase: synthesis, molecular modeling, and biological studies. *J. Med. Chem.* **2011**, *54*, 1401–1420.

- (20) Bookser, B. C.; Matelich, M. C.; Ollis, K.; Ugarkar, B. G. Adenosine kinase inhibitors. 4. 6,8-Disubstituted purine nucleoside derivatives. Synthesis, conformation, and enzyme inhibition. *J. Med. Chem.* **2005**, *48*, 3389–3399.

- (21) Jarvis, M. F.; Yu, H.; McGaraughty, S.; Wismer, C. T.; Mikusa, J.; Zhu, C.; Chu, K.; Kohlhaas, K.; Cowart, M.; Lee, C.-H.; Stewart, A. O.; Cox, B. F.; Polakowski, J.; Kowaluk, E. A. Analgesic and anti-inflammatory effects of A-286501, a novel orally active adenosine kinase inhibitor. *Pain* **2002**, *96*, 107–118.

- (22) McGaraughty, S.; Chu, K. L.; Wismer, C. T.; Mikusa, J.; Zhu, C. Z.; Cowart, M.; Kowaluk, E.; Jarvis, M. F. Effects of A-134974, a novel adenosine kinase inhibitor, on carrageenan-induced inflammatory hyperalgesia and locomotor activity in rats: evaluation of the sites of action. *J. Pharmacol. Exp. Ther.* **2001**, *296*, S01–S09.

- (23) Tatlisumak, T.; Takano, K.; Carano, R. A. D.; Miller, L. P.; Foster, A. C.; Fisher, M.; Hsu, C. Y.; Lin, W. Delayed treatment with an adenosine kinase inhibitor, GP683, attenuates infarct size in stroke. *Stroke* **1998**, *29*, 1952–1958.

- (24) Malnuit, V.; Slavětínská, L. P.; Nauš, P.; Džubák, P.; Hajdúch, M.; Stolaříková, J.; Snášel, J.; Pichová, I.; Hocek, M. 2-Substituted 6-

(het)aryl-7-deazapurine ribonucleosides: Synthesis, inhibition of adenosine kinases, and antimycobacterial activity. *ChemMedChem* **2015**, *10*, 1079–1093.

(25) Long, M. C.; Shaddix, S. C.; Moukha-Chafiq, O.; Maddry, J. A.; Nagy, L.; Parker, W. B. Structure–activity relationship for adenosine kinase from *Mycobacterium tuberculosis*: II. Modifications to the ribofuranosyl moiety. *Biochem. Pharmacol.* **2008**, *75*, 1588–1600.

(26) McGaraughty, S.; Cowart, M.; Jarvis, M. F.; Berman, R. F. Anticonvulsant and antinociceptive actions of novel adenosine kinase inhibitors. *Curr. Top. Med. Chem.* **2005**, *5*, 43–58.

(27) Cronstein, B. N.; Naime, D.; Firestein, G. The antiinflammatory effects of an adenosine kinase inhibitor are mediated by adenosine. *Arthritis Rheum.* **1995**, *38*, 1040–1045.

(28) Lee, J. K.; Won, J. S.; Singh, A. K.; Singh, I. Adenosine kinase inhibitor attenuates the expression of inducible nitric oxide synthase in glial cells. *Neuropharmacology* **2005**, *48*, 151–160.

(29) Cottam, H. B.; Wasson, D. B.; Shih, H. C.; Raychaudhuri, A.; Di Pasquale, G.; Carson, D. A. New adenosine kinase inhibitors with oral antiinflammatory activity: synthesis and biological evaluation. *J. Med. Chem.* **1993**, *36*, 3424–3430.

(30) Annes, J. P.; Ryu, J. H.; Lam, K.; Carolan, P. J.; Utz, K.; Hollister-Lock, J.; Arvanites, A. C.; Rubin, L. L.; Weir, G.; Melton, D. A. Adenosine kinase inhibition selectively promotes rodent and porcine islet β -cell replication. *Proc. Natl. Acad. Sci. U. S. A.* **2012**, *109*, 3915–3920.

(31) García-Villafranca, J.; Castro, J. Effects of 5-iodotubercidin on hepatic fatty acid metabolism mediated by the inhibition of acetyl-CoA carboxylase. *Biochem. Pharmacol.* **2002**, *63*, 1997–2000.

(32) Marquez, V. E.; Siddiqui, M. A.; Ezzitouni, A.; Russ, P.; Wang, J.; Wagner, R. W.; Matteucci, M. D. Nucleosides with a twist. Can fixed forms of sugar ring pucker influence biological activity in nucleosides and oligonucleotides? *J. Med. Chem.* **1996**, *39*, 3739–3747.

(33) Maruoka, H.; Barrett, M. O.; Ko, H.; Tosh, D. K.; Melman, A.; Burianek, L. E.; Balasubramanian, R.; Berk, B.; Costanzi, S.; Harden, T. K.; Jacobson, K. A. Pyrimidine ribonucleotides with enhanced selectivity as P2Y₆ receptor agonists: Novel 4-alkyloxymino, (S)-methanocarba, and 5'-triphosphate γ -ester modifications. *J. Med. Chem.* **2010**, *53*, 4488–4501.

(34) Snášel, J.; Nauš, P.; Dostál, J.; Hnízda, A.; Fanfrlík, J.; Brynda, J.; Bourderioux, A.; Dušek, M.; Dvořáková, H.; Stolaříková, J.; Zábanská, H.; Pohl, R.; Konečný, P.; Džubák, P.; Votruba, I.; Hajdúch, M.; Rezáčová, P.; Veverka, V.; Hocek, M.; Pichová, I. Structural basis for inhibition of mycobacterial and human adenosine kinase by 7-substituted 7-(het)aryl-7-deazaadenine ribonucleosides. *J. Med. Chem.* **2014**, *57*, 8268–8279.

(35) (a) Schelling, P.; Claus, M. T.; Johner, R.; Marquez, V. E.; Schulz, G. E.; Scapozza, L. Biochemical and structural characterization of (South)-methanocarbothymidine that specifically inhibits growth of herpes simplex virus type 1 thymidine kinase-transduced osteosarcoma cells. *J. Biol. Chem.* **2004**, *279*, 32832–32838. (b) Marquez, V. E.; Choi, Y.; Comin, M. J.; Russ, P.; George, C.; Huleihel, M.; Ben-Kasus, T.; Agbaria, R. Understanding how the herpes thymidine kinase orchestrates optimal sugar and nucleobase conformations to accommodate its substrate at the active site: A chemical approach. *J. Am. Chem. Soc.* **2005**, *127*, 15145–15150. (c) Sun, G.; Voigt, J. H.; Filippov, I. V.; Marquez, Y. E.; Nicklaus, M. C. PROSIT: Pseudo-Rotational Online Service and Interactive Tool, applied to a conformational survey of nucleosides and nucleotides. *J. Chem. Inf. Comp. Sci.* **2004**, *44*, 1752–1762.

(36) Muchmore, S. W.; Smith, R. A.; Stewart, A. O.; Cowart, M. D.; Gomtshyan, A.; Matulenko, M. A.; Yu, H.; Severin, J. M.; Bhagwat, S. S.; Lee, C. H.; Kowaluk, E. A.; Jarvis, M. F.; Jakob, C. L. Crystal structures of human adenosine kinase inhibitor complexes reveal two distinct binding modes. *J. Med. Chem.* **2006**, *49*, 6726–6731.

(37) Mathews, I. I.; Erion, M. D.; Ealick, S. E. Structure of human adenosine kinase at 1.5 Å resolution. *Biochemistry* **1998**, *37*, 15607–15620.

(38) Joshi, B. V.; Melman, A.; Mackman, R. L.; Jacobson, K. A. Synthesis of ethyl (1S,2R,3S,4S,5S)-2,3-O-(isopropylidene)-4-hydroxy-

bicyclo[3.1.0]hexane-carboxylate from L-ribose: A versatile chiral synthon for preparation of adenosine and P2 receptor ligands. *Nucleosides, Nucleotides Nucleic Acids* **2008**, *27*, 279–291.

(39) Melman, A.; Zhong, M.; Marquez, V. E.; Jacobson, K. A. Synthesis of enantiomerically pure (S)-methanocarbaribo uracil nucleoside derivatives for use as antiviral agents and P2Y receptor ligands. *J. Org. Chem.* **2008**, *73*, 8085–8088.

(40) Smith, D. E.; Marquez, I.; Lokensgard, M. E.; Rheingold, A. L.; Hecht, D. A.; Gustafson, J. L. Exploiting atropisomerism to increase the target selectivity of kinase inhibitors. *Angew. Chem., Int. Ed.* **2015**, *54*, 11754–11759.

(41) Boyer, S. H.; Ugarkar, B. G.; Solbach, J.; Kopcho, J.; Matelich, M. C.; Ollis, K.; Gomez-Galeno, J. E.; Mendonca, R.; Tsuchiya, M.; Nagahisa, A.; Nakane, M.; Wiesner, J. B.; Erion, M. D. Adenosine kinase inhibitors. 5. Synthesis, enzyme inhibition, and analgesic activity of diaryl-erythro-furanosyltubercidin analogues. *J. Med. Chem.* **2005**, *48*, 6430–6441.

(42) Toti, K. S.; Derudas, M.; Pertusati, F.; Sinnaeve, D.; Van den Broeck, F.; Margamuljana, L.; Martins, J. C.; Herdewijn, P.; Balzarini, J.; McGuigan, C.; Van Calenbergh, S. Synthesis of an apionucleoside family and discovery of a prodrug with anti-HIV activity. *J. Org. Chem.* **2014**, *79*, 5097–5112.

(43) Ugarkar, B. G.; DaRe, J. M.; Kopcho, J. J.; Browne, C. E., III; Schanzer, J. M.; Wiesner, J. B.; Erion, M. D. Adenosine kinase inhibitors. 1. Synthesis, enzyme inhibition, and antiseizure activity of 5-iodotubercidin analogues. *J. Med. Chem.* **2000**, *43*, 2883–2893.

(44) Epp, J. B.; Widlanski, T. S. Facile preparation of nucleoside-5'-carboxylic acids. *J. Org. Chem.* **1999**, *64*, 293–295.

(45) Tosh, D. K.; Padia, J.; Salvemini, D.; Jacobson, K. A. Efficient, large-scale synthesis and preclinical studies of MRS5698, a highly selective A₃ adenosine receptor agonist that protects against chronic neuropathic pain. *Purinergic Signalling* **2015**, *11*, 371–387.

(46) Bhutoria, S.; Ghoshal, N. Deciphering ligand dependent degree of binding site closure and its implication in inhibitor design: A modeling study on human adenosine kinase. *J. Mol. Graphics Modell.* **2010**, *28*, 577–591.

(47) Dong, L.; Shi, J.; Wang, J.; Liu, Y. Theoretical studies on the conformational change of adenosine kinase induced by inhibitors. *Int. J. Quantum Chem.* **2011**, *111*, 3980–3990.

(48) Hernandez, S.; Ford, H., Jr.; Marquez, V. E. Is the anomeric effect an important factor in the rate of adenosine deaminase catalyzed hydrolysis of purine nucleosides? A direct comparison of nucleoside analogues constructed on ribose and carbocyclic templates with equivalent heterocyclic bases selected to promote hydration. *Bioorg. Med. Chem.* **2002**, *10*, 2723–2730.

(49) Schaddelee, M. P.; Read, K. D.; Cleypool, C. G.; IJzerman, A. P.; Danhof, M.; de Boer, A. G. Brain penetration of synthetic adenosine A₁ receptor agonists in situ: role of the rENT1 nucleoside transporter and binding to blood constituents. *Eur. J. Pharm. Sci.* **2005**, *24*, 59–66.

(50) Pardridge, W. M. Blood–brain barrier endogenous transporters as therapeutic targets: a new model for small molecule CNS drug discovery. *Expert Opin. Ther. Targets* **2015**, *19*, 1059–1072.

(51) Sinclair, C. J. D.; Powell, A. E.; Xiong, W.; LaRivière, C. G.; Baldwin, S. A.; Cass, C. E.; Young, J. D.; Parkinson, F. E. Nucleoside transporter subtype expression: effects on potency of adenosine kinase inhibitors. *Br. J. Pharmacol.* **2001**, *134*, 1037–1044.

(52) Lee, K.; Cass, C.; Jacobson, K. A. Synthesis using ring closure metathesis and effect on nucleoside transport of a (N)-methanocarba S-(4-nitrobenzyl)thioinosine derivative. *Org. Lett.* **2001**, *3*, 597–599.

(53) Damaraju, V. L.; Mowles, D.; Smith, K. M.; Yao, S. Y.; Young, J. D.; Marquez, V. E.; Cass, C. E. Influence of sugar ring conformation on the transportability of nucleosides by human nucleoside transporters. *ChemBioChem* **2011**, *12*, 2774–2778.

(54) Mato, J. M.; Martínez-Chantar, M. L.; Lu, S. C. Methionine metabolism and liver disease. *Annu. Rev. Nutr.* **2008**, *28*, 273–293.

(55) Besnard, J.; Ruda, G. F.; Setola, V.; Abecassis, K.; Rodriguez, R. M.; Huang, X. P.; Norval, S.; Sassano, M. F.; Shin, A. I.; Webster, L. A.; Simeons, F. R.; Stojanovski, L.; Prat, A.; Seidah, N. G.; Constam, D. B.; Bickerton, G. R.; Read, K. D.; Wetsel, W. C.; Gilbert, I. H.; Roth, B.

- L.; Hopkins, A. L. Automated design of ligands to polypharmacological profiles. *Nature* **2012**, *492*, 215–220.
- (56) *Maestro*, version 10.3; Schrödinger, LLC: New York, 2015.
- (57) *Jaguar*, version 8.9; Schrödinger, LLC: New York, 2015.
- (58) Bernstein, F. C.; Koetzle, T. F.; Williams, G. J.; Meyer, E. E., Jr.; Brice, M. D.; Rodgers, J. R.; Kennard, O.; Shimanouchi, T.; Tasumi, M. The protein data bank: A computer-based archival file for macromolecular structures. *J. Mol. Biol.* **1977**, *112*, 535–542.
- (59) Sastry, G. M.; Adzhigirey, M.; Day, T.; Annabhimoju, R.; Sherman, W. Protein and ligand preparation: parameters, protocols, and influence on virtual screening enrichments. *J. Comput.-Aided Mol. Des.* **2013**, *27*, 221–234.
- (60) *Glide*, version 6.8; Schrödinger, LLC: New York, 2015.
- (61) *Prime*, version 4.1; Schrödinger, LLC: New York, 2015.
- (62) Harder, E.; Damm, W.; Maple, J.; Wu, C.; Reboul, M.; Xiang, J. Y.; Wang, L.; Lupyan, D.; Dahlgren, M. K.; Knight, J. L.; Kaus, J. W.; Cerutti, D. S.; Krilov, G.; Jorgensen, W. L.; Abel, R.; Friesner, R. A. OPLS3: A force field providing broad coverage of drug-like small molecules and proteins. *J. Chem. Theory Comput.* **2016**, *12*, 281–296.
- (63) Harvey, M.; Giupponi, G.; De Fabritiis, G. ACEMD: Accelerated molecular dynamics simulations in the microseconds timescale. *J. Chem. Theory Comput.* **2009**, *5*, 1632–1639.
- (64) Case, D.; Babin, V.; Berryman, J.; Betz, R.; Cai, Q.; Cerutti, D.; Cheatham Iii, T.; Darden, T.; Duke, R.; Gohlke, H. *Amber14*, 2014; <http://ambermd.org/> (accessed May 2016).
- (65) Wang, J.; Wolf, R. M.; Caldwell, J. W.; Kollman, P. A.; Case, D. A. Development and testing of a general amber force field. *J. Comput. Chem.* **2004**, *25*, 1157–1174.
- (66) Frisch, M. J.; Trucks, G. W.; Schlegel, H. B.; Scuseria, G. E.; Robb, M. A.; Cheeseman, J. R.; Scalmani, G.; Barone, V.; Mennucci, B.; Petersson, G. A.; Nakatsuji, H.; Caricato, M.; Li, X.; Hratchian, H. P.; Izmaylov, A. F.; Bloino, J.; Zheng, G.; Sonnenberg, J. L.; Hada, M.; Ehara, M.; Toyota, K.; Fukuda, R.; Hasegawa, J.; Ishida, M.; Nakajima, T.; Honda, Y.; Kitao, O.; Nakai, H.; Vreven, T.; Montgomery, J. A.; Peralta, J. E.; Ogliaro, F.; Bearpark, M.; Heyd, J. J.; Brothers, E.; Kudin, K. N.; Staroverov, V. N.; Kobayashi, R.; Normand, J.; Raghavachari, K.; Rendell, A.; Burant, J. C.; Iyengar, S. S.; Tomasi, J.; Cossi, M.; Rega, N.; Millam, J. M.; Klene, M.; Knox, J. E.; Cross, J. B.; Bakken, V.; Adamo, C.; Jaramillo, J.; Gomperts, R.; Stratmann, R. E.; Yazyev, O.; Austin, A. J.; Cammi, R.; Pomelli, C.; Ochterski, J. W.; Martin, R. L.; Morokuma, K.; Zakrzewski, V. G.; Voth, G. A.; Salvador, P.; Dannenberg, J. J.; Dapprich, S.; Daniels, A. D.; Farkas, Foresman, J. B.; Ortiz, J. V.; Cioslowski, J.; Fox, D. J. *Gaussian 09*, revision B.01; Gaussian, Inc.: Wallingford, CT, 2009.
- (67) Jorgensen, W. L.; Chandrasekhar, J.; Madura, J. D.; Impey, R. W.; Klein, M. L. Comparison of simple potential functions for simulating liquid water. *J. Chem. Phys.* **1983**, *79*, 926–935.
- (68) Loncharich, R. J.; Brooks, B. R.; Pastor, R. W. Langevin dynamics of peptides: the frictional dependence of isomerization rates of *N*-acetylalanyl-*N'*-methylamide. *Biopolymers* **1992**, *32*, 523–535.
- (69) Berendsen, H. J. C.; Postma, J. P. M.; van Gunsteren, W. F.; DiNola, A.; Haak, J. R. Molecular dynamics with coupling to an external bath. *J. Chem. Phys.* **1984**, *81*, 3684–3690.
- (70) Kräutler, V.; Van Gunsteren, W. F.; Hünenberger, P. H. A Fast SHAKE algorithm to solve distance constraint equations for small molecules in molecular dynamics simulations. *J. Comput. Chem.* **2001**, *22*, 501–508.
- (71) Essmann, U.; Perera, L.; Berkowitz, M. L.; Darden, T.; Lee, H.; Pedersen, L. G. A. Smooth particle mesh Ewald method. *J. Chem. Phys.* **1995**, *103*, 8577–8593.
- (72) Humphrey, W.; Dalke, A.; Schulten, K. VMD - Visual molecular dynamics. *J. Mol. Graphics* **1996**, *14*, 33–38.
- (73) Phillips, J. C.; Braun, R.; Wang, W.; Gumbart, J.; Tajkhorshid, E.; Villa, E.; Chipot, C.; Skeel, R. D.; Kale, L.; Schulten, K. Scalable molecular dynamics with NAMD. *J. Comput. Chem.* **2005**, *26*, 1781–1802.
- (74) Sabbadin, D.; Ciancetta, A.; Moro, S. Bridging molecular docking to membrane molecular dynamics to investigate GPCR–ligand recognition: The human A_{2A} adenosine receptor as a key study. *J. Chem. Inf. Model.* **2014**, *54*, 169–183.
- (75) Williams, T.; Kelley, C. *Gnuplot 4.6: An Interactive Plotting Program*, version 4.6.6, 2014; <http://gnuplot.info> (accessed May 2016).
- (76) Altona, C.; Sundaralingam, M. Conformational analysis of the sugar ring in nucleosides and nucleotides. A new description using the concept of pseudorotation. *J. Am. Chem. Soc.* **1972**, *94*, 8205–8212.
- (77) van der Spoel, D.; Lindahl, E.; Hess, B.; GROMACS Development Team. *GROMACS User Manual*, version 4.6.5, 2013; www.gromacs.org.
- (78) Hess, B.; Kutzner, C.; van der Spoel, D.; Lindahl, E. GROMACS 4: Algorithms for highly efficient, load-balanced, and scalable molecular simulation. *J. Chem. Theory Comput.* **2008**, *4*, 435–447.
- (79) Girdlestone, C.; Hayward, S. The DynDom3D webserver for the analysis of domain movements in multimeric proteins. *J. Comput. Biol.* **2015**, *23*, 21–26.
- (80) Datta, R.; Das, I.; Sen, B.; Chakraborty, A.; Adak, S.; Mandal, C.; Datta, A. K. Homology-model-guided site-specific mutagenesis reveals the mechanisms of substrate binding and product-regulation of adenosine kinase from *Leishmania donovani*. *Biochem. J.* **2006**, *394*, 35–42.